Acta Cryst. (1996). B52, 38–53

Modulated Structure of $Bi_2Sr_2CaCu_2O_{8+\delta}$, A High-$T_c$ Superconductor with Monoclinic Symmetry

ROMAN E. GLADYSHEVSKII* AND RENÉ FLÜKIGER

Département de Physique de la Matière Condensée, Université de Genève, 24 quai Ernest-Ansermet, CH-1211 Genève 4, Switzerland

(*Received 24 March 1995; accepted 25 May 1995*)

Abstract

The structure of the bismuth strontium calcium cuprate $Bi_{2.09}Sr_{1.90}Ca_{1.00}Cu_2O_{8.22}$ ($T_c = 90$ K) was studied by single-crystal X-ray diffraction. A two-component modulation vector was found with respect to the *C*-centred orthorhombic cell of the average structure [$a = 5.4112(7)$, $b = 30.873(7)$, $c = 5.4161(20)$ Å, $\mathbf{q} = 0.21\mathbf{c}^* + 0.14\mathbf{b}^*$]. Refinement was performed in a ninefold supercell [$M_r = 902$, monoclinic, *mS*548-0.4, *Cc* (No. 9), $a = 37.754(7)$, $b = 5.4109(8)$, $c = 41.070(9)$ Å, $\beta = 103.58(2)°$, $V = 8155(2)$ Å^3, $Z = 36$, $D_x = 6.61$ Mg m^{-3}] to $wR = 0.057$. As in orthorhombic $Bi_2Sr_2CaCu_2O_{8+\delta}$, the structure of this new monoclinic variant contains perovskite-derived slabs delimited by a BiO layer on each side. All metal atoms show a transverse displacement wave which has the largest amplitude for the Cu and Ca atoms. In addition, the Bi and Sr atoms are displaced longitudinally. Bi-rich regions with a distorted rocksalt-type atom arrangement and Bi-poor regions with chains of corner-linked BiO_3 ψ-tetrahedra are formed. One additional oxygen site per translation unit of the modulation wave was detected in the Bi-poor regions of the chains, giving the composition Bi_9O_{10}. Approximately 10% of Bi substitution was found on the Ca sites, but no clear indication of preferential sites was observed. A partial substitution by Ca was refined at Sr sites situated near the regions where the additional O atoms are located. The monoclinic symmetry corresponds to a systematic shift of the modulation waves of consecutive slabs by $\pi/9$ with respect to orthorhombic $Bi_2Sr_2CaCu_2O_{8+\delta}$.

1. Introduction

Since the discovery of superconductivity in the Bi–Sr–Ca–Cu–O system (Maeda, Tanaka, Fukotomi & Asano, 1988), there has been a large amount of literature on Bi-based high-T_c superconductors. If the average structures of the superconducting compounds were readily identified, the real structures turned out to be more complicated than expected, combining displacive and substitutional modulation. The presence of both heavy and light elements makes it difficult to study the structures by X-ray diffraction, whereas the strong two-dimensional character makes it difficult to obtain single crystals large enough for neutron diffraction studies.

Compounds of the general formula $Bi_2Sr_2Ca_{n-1}Cu_nO_{4+2n+\delta}$ crystallize with structures which may be considered as built up of two types of alternating slabs: a rocksalt-derived slab formed by two BiO layers and a perovskite-derived slab containing $n$$CuO_2$ layers. The unit cells of the average structures are pseudo-tetragonal with $a \approx b \approx 5.4$ and $c \approx 24.6$, 30.9 and 37.0 Å for $n = 1$, 2 and 3, respectively, but the real symmetry is lower. An incommensurate modulation in the direction of one of the short cell vectors with a translation periodicity of approximately 4.7*b* has been reported for all unsubstituted members of the structure series. The translation periodicity of the modulation vector with respect to the cell parameter of the orthorhombic cell does not vary significantly within the Sr–Ca homogeneity range (Niu, Fukushima, Takeno, Nakamura & Ando, 1989) and remains stable down to 8 K (Takenaka, Kamigaki, Terauchi & Katsui, 1989; Patterson *et al.*, 1990; Beskrovnyi, Dlouhá, Jirák & Vratislav, 1990). However, when Ca is substituted by a trivalent rare earth element it progressively decreases to 4*b* (Niu, Fukushima, Takeno, Nakamura & Ando, 1989; Onozuka & Hirotsu, 1994), whereas when Bi is replaced by Pb the modulation periodicity increases to 10*b* (Calestani, Francesconi, Salsi, Andreetti & Migliori, 1992). Substitution of Cu by a transition metal in some cases leads to the formation of a commensurate superstructure (Le Page, McKinnon, Tarascon & Barboux, 1989; Tarascon, Le Page & McKinnon, 1990).

The average structure of the compound $Bi_2Sr_2CaCu_2O_{8+\delta}$ has been reported by several authors in space group *Cccm* with the unit-cell parameters $a \approx c \approx 5.4$ and $b \approx 30.9$ Å, the published data usually referring to the non-standard settings *Amaa* or *Bbmb*. Other authors claim that better agreement is obtained in the non-centrosymmetric subgroup *Ccc*2 (*A*2*aa*, *Bb*2*b*).

A one-dimensional modulation was reported by Gao, Lee, Coppens, Subramanian & Sleight (1988). A refinement in four-dimensional superspace group L_{11-1}^{Cccm} was carried out by Yamamoto *et al.* (1990), who combined powder X-ray and neutron time-of-flight

diffraction data. The refined composition, $Bi_{2.33}Sr_{1.4}Ca_{1.3}Cu_2O_9$, contains a surprisingly high amount of oxygen. Petricek, Gao, Lee & Coppens (1990) preferred the non-centrosymmetric superspace group L_{111}^{Ccc2} for their refinement on single-crystal X-ray data. These authors also report extra O atoms, which they consider to be responsible for the modulation. Kan & Moss (1992) report a refinement in the same space group, but from their X-ray diffraction data cannot confirm the presence of additional O atoms. They attribute the origin of the modulation to a mismatch between the rocksalt and the perovskite-derived slabs. Gao, Coppens, Cox & Moodenbaugh (1993) combine neutron powder diffraction data with the diffraction data of Petricek, Gao, Lee & Coppens (1990) and confirm the previously reported results.

Several refinements in supercells have been performed by approximating the modulation periodicity to five times the translation period of the average lattice. Horiuchi, Maeda, Tanaka & Matsui (1988) proposed a superstructure in space group *Cmcm* from high-resolution transmission electron-microscope studies. Le Page, McKinnon, Tarascon & Barboux (1989) refined the closely related structure of $Bi_{10}Sr_{15}Fe_{10}O_{46}$ in space group *C*222 from single-crystal X-ray diffraction data, inserting one additional O atom per formula unit into the BiO layers of this apparently truly commensurate structure with a fivefold supercell. Calestani, Rizzoli, Francesconi & Andreetti (1989) refined the structure of the Cu-based compound from single-crystal X-ray diffraction data in a primitive cell of the same volume, in space group *Pnnn*. Levin, Smolin & Shepelev (1994) chose the same space group but, contrary to Calestani, Rizzoli, Francesconi & Andreetti (1989), observed additional oxygen sites and vacancies on some Sr sites. Beskrovnyi, Dlouhá, Jirák, Vratislav & Pollert (1990) and Beskrovnyi, Dlouhá, Jirák & Vratislav (1990) used a 19-fold unit cell, assuming that the translation period of the modulation vector with respect to the cell parameter of the average structure is equal to 4.75. From single-crystal neutron diffraction data they detected additional oxygen sites, as well as vacancies on the Sr sites. Several authors have reported that the real symmetry of the phase is probably monoclinic or lower (*e.g.* Kan & Moss, 1992; Zhigadlo, 1994).

We report here on a new structural variant of $Bi_2Sr_2CaCu_2O_{8+\delta}$. As for the monoclinic so-called *I*- or *A*-variant of $Bi_2Sr_2CuO_{6+\delta}$ (Onoda & Sato, 1988; Leligny, Durčok, Labbe, Ledesert & Raveau, 1992; Beskrovnyi, Durčok, Hejtmánek, Jirák, Pollert & Shelkova, 1994), the monoclinic symmetry corresponds to a systematic phase shift of the modulation wave.

2. Experimental

A detailed account of the sample preparation is given elsewhere (Tsukamoto *et al.*, 1994). Single crystals were prepared by the travelling-solvent floating-zone method from a sample of nominal composition $Bi_{2.16}Sr_{1.94}Ca_{1.04}Cu_2O_x$. A fragment ($0.176 \times 0.176 \times 0.012$ mm) was cut from a large plate-like crystal, for which a T_c^{onset} of 90 K was measured. The specific heat up to 14 T and the magnetization of a single crystal of the same sample have been reported in a separate paper (Junod *et al.*, 1994). Experimental details are given in Table 1.

Table 1. *Experimental details*

Crystal data	
Chemical formula	$Bi_{2.09}Sr_{1.90}Ca_{1.00}Cu_2O_{8.22}$
Chemical formula weight	902.93
Cell setting	Monoclinic
Space group	*Cc*
a (Å)	37.754 (7)
b (Å)	5.4109 (8)
c (Å)	41.070 (9)
β (°)	103.58 (2)
V (Å^3)	8155 (2)
Z	36
D_x (Mg m^{-3})	6.61
Radiation type	Mo $K\alpha$
Wavelength (Å)	0.71073
No. of reflections for cell parameters	46
θ range (°)	11–23.5
μ (mm^{-1})	56.740
Temperature (K)	293
Crystal form	Plate
Crystal size (mm)	$0.176 \times 0.176 \times 0.012$
Crystal colour	Black
Data collection	
Diffractometer	Stoe Stadi 4
Data collection method	ω-2θ
Absorption correction	Analytical
T_{min}	0.011
T_{max}	0.506
No. of measured reflections	14 692
No. of independent reflections	7227
R_{int}	0.223
θ_{max} (°)	25
Range of *h*, *k*, *l*	$0 \rightarrow h \rightarrow 44$ $0 \rightarrow k \rightarrow 6$ $-48 \rightarrow l \rightarrow 48$
No. of standard reflections	2
Frequency of standard reflections	60
Intensity decay (%)	0.5
Refinement	
Refinement on	*F*
R	0.144
wR	0.057
S	1.09
No. of reflections used in refinement	7227
No. of parameters used	579
Weighting scheme	$w = 1/\sigma^2(F)$
$(\Delta/\sigma)_{max}$	0.4
$\Delta\rho_{max}$ (e Å^{-3})	11.6
$\Delta\rho_{min}$ (e Å^{-3})	9.6
Extinction method	Zachariasen (1968)
Extinction coefficient	0.075 (7)
Source of atomic scattering factors	*International Tables for X-ray Crystallography* (1974, Vol. IV)

The single crystal was mounted on a Stoe-Stadi 4 automatic four-circle diffractometer equipped with Mo$K\alpha$ radiation ($\lambda = 0.71073$ Å, graphite monochro-

Table 2. *Indexation of the 25 initially detected diffraction peaks*

(*a*) Based on the *C*-centred orthorhombic cell of the average structure, (*b*) considering a fourth translation vector (superspace group P_1^{Cc}) and (*c*) based on a monoclinic *C*-centred ninefold supercell. The relative intensities are listed in the last column.

(*a*) $a = 5.41$ Å, $b = 30.87$ Å, $c = 5.42$ Å			(*b*) $a = 30.87$ Å, $b = 5.41$ Å, $c = 5.42$ Å, $\beta = 90.1°$, $\mathbf{q} = 0.11\mathbf{c}^* - 0.57\mathbf{a}^*$				(*c*) $a = 37.75$ Å, $b = 5.41$ Å, $c = 41.07$ Å, $\beta = 103.6°$			
h	*k*	*l*	*h*	*k*	*l*	*m*	*h*	*k*	*l*	*I*
0	0	2	0	0	2	0	8	0	10	100
1	−7	1	7	1	1	0	−3	−1	12	49
−1	−7	−1	7	−1	−1	0	−11	1	2	47
2	−10	0	10	2	0	0	−10	−2	10	28
−1	−3	−1	3	−1	−1	0	−7	1	−2	25
1	−3	1	3	1	1	0	1	−1	8	25
−1	−9	−1	9	−1	−1	0	−13	1	4	15
0	−8	0	8	0	0	0	−8	0	8	11
1	−15	1	15	1	1	0	−11	−1	20	11
−1	−15	−1	15	−1	−1	0	−19	1	10	10
−2	−12	0	12	−2	0	0	−12	2	12	10
2	−12	0	12	2	0	0	−12	−2	12	9
−2	−8	0	8	−2	0	0	−8	2	8	9
−2	−8	−2	8	−2	−2	0	−16	2	−2	8
3	−3	1	3	3	1	0	1	−3	8	6
0	−11.14	−2.21	10	0	−2	−2	−20	0	0	6
0	0.85	1.79	−2	0	2	−2	8	0	8	5
2	−1.15	1.79	0	2	2	−2	6	−2	10	4
0	−10.87	2.21	12	0	2	2	−2	0	22	4
0	−6.87	2.21	8	0	2	2	2	0	18	3
2	−6	0	6	2	0	0	−6	−2	6	3
1	−9	−1	9	1	−1	0	−13	−1	4	2
−2	−8.86	−1.79	10	−2	−2	2	−16	2	0	2
0	−8.85	−1.79	10	0	−2	2	−16	0	0	2
1	−15.85	−0.79	17	1	−1	2	−19	−1	12	1

mator). Of the 25 initially collected reflections, the relative intensities of which are listed in Table 2, only 17 had integer indexes referring to the orthorhombic cell of the average structure. The remaining reflections could be indexed considering a fourth translation vector, $\mathbf{q} = 0.21\mathbf{c}_o^* + 0.14\mathbf{b}_o^*$, which has a small but significant component along $\mathbf{b}^*$ of the orthorhombic cell. The second column of Table 2 contains indexes based on a monoclinic cell, obtained by the following transformation: $\mathbf{a}_m = -\mathbf{b}_o$, $\mathbf{b}_m = \mathbf{a}_o$, $\mathbf{c}_m = \mathbf{c}_o$, and a fourth vector $\mathbf{q}' = 0.11\mathbf{c}_m^* - 0.57\mathbf{a}_m^*$, which respects the extinction

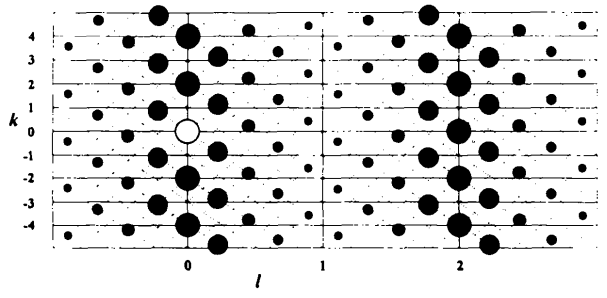

Fig. 1. Superposition of the translation lattices corresponding to the orthorhombic subcell (solid lines) and the ninefold monoclinic supercell (dotted lines) in reciprocal space (0*kl* section, referring to the orthorhombic lattice). Large black circles indicate the main reflections; four orders of satellites are shown, smaller circles correspond to higher order.

Table 3. *Comparison of refinements in the subcell and supercell for* $Bi_2Sr_2CaCu_2O_{8+\delta}$

	Subcell (orthorhombic)	Supercell (monoclinic)
Reflections for unit cell (2θ range (°))	27(24–47)	46(22–47)
hkl with antireflections	$0 \le h \le 6$ $0 \le k \le 36$ $0 \le l \le 6$	$0 \le h \le 44$ $0 \le k \le 6$ $-48 \le l \le 48$
Collected reflections	1830	14 692
Unique reflections	458	7227
Reflections with $\lvert F_{rel}\rvert > 3\sigma(\lvert F_{rel}\rvert)$	276	1707
Refined parameters	55	579
Atom sites	9	137
U anisotropic	Bi, Sr, Cu, Ca	Bi
U isotropic	O	Sr, Cu, Ca, O
Extinction *G*	0.08 (3)	0.075 (7)
S	1.44	1.09
wR, $w = 1/\sigma^2(\lvert F_{rel}\rvert)$	0.026	0.057

rules for superspace group P_1^{Cc}. It is, however, possible to index the same reflections in three-dimensional space in a satisfactory way, making the approximation $\mathbf{q} = 2\mathbf{c}_o^*/9 + \mathbf{b}_o^*/9$. The indexation based on a *C*-centred monoclinic ninefold supercell taking account of this vector is given in the third column of Table 2. Fig. 1 shows the translation lattices corresponding to the orthorhombic subcell (solid lines) and the monoclinic supercell (dotted lines) in reciprocal space (0*kl* section, referring to the orthorhombic lattice). The large black circles represent the main reflections, *i.e.* those which can

Table 4. *Fractional atomic coordinates, isotropic or equivalent displacement parameters ($Å^2 \times 10^2$) and population parameters (PP) in the average structure of $Bi_{2.10(1)}Sr_{1.78(6)}Ca_{1.12(7)}Cu_2O_8$, space group Ccc2*

The displacement parameters were refined anisotropically for the metal-atom sites, isotropically for the O sites.

$$U_{eq} = (1/3)\sum_i \sum_j U_{ij} a_i^* a_j^* \mathbf{a}_i \cdot \mathbf{a}_j.$$

		x	y	z	$U_{iso/eq}$	PP
Bi(1)	8(*d*)	0.2264 (3)	0.0546 (2)	0.455 (2)	3.07 (7)	0.552 (9)
Bi(2)	8(*d*)	0.2264 (3)	0.0491 (2)	0.559 (3)	3.07 (7)	0.448 (9)
Sr	8(*d*)	0.2504 (7)	0.1410 (2)	0.994 (3)	4.5 (1)	0.89 (3) Sr + 0.11 (3) Ca
Cu	8(*d*)	0.2488 (8)	0.1968 (2)	0.500 (3)	3.8 (1)	
Ca	4(*c*)	1/4	1/4	0.999 (4)	3.7 (3)	0.90 (1) Ca + 0.10 (1) Bi
O(1)	8(*d*)	0.141 (7)	0.0502 (12)	0.190 (3)	7.3 (8)	
O(2)	8(*d*)	0.280 (5)	0.1196 (9)	0.574 (3)	5.1 (7)	
O(3)	8(*d*)	0.001 (8)	0.1972 (7)	0.246 (5)	2.6 (5)	
O(4)	8(*d*)	0.006 (7)	0.2938 (5)	0.249 (5)	1.4 (4)	

Constraints: x[Bi(2)] = x[Bi(1)], U_{ij}[Bi(2)] = U_{ij}[Bi(1)], PP[Bi(1)] + PP[Bi(2)] = 1.

Table 5. *Anisotropic displacement parameters ($Å^2 \times 10^2$) of the metal-atom sites in the average structure of $Bi_{2.10}Sr_{1.78}Ca_{1.12}Cu_2O_8$, space group Ccc2*

	U_{11}	U_{22}	U_{33}	U_{12}	U_{13}	U_{23}
Bi	1.59 (8)	3.2 (1)	4.4 (2)	0.3 (1)	−0.7 (3)	2.0 (2)
Sr	0.9 (2)	6.6 (3)	6.0 (3)	0.5 (3)	0.9 (4)	0.5 (6)
Cu	1.0 (2)	9.1 (3)	1.4 (1)	0.6 (3)	−0.1 (3)	0.7 (4)
Ca	2.1 (4)	7.6 (6)	1.5 (3)	0.2 (5)	0	0

U_{ij}[Bi] = U_{ij}[Bi(1)] = U_{ij}[Bi(2)].

be indexed based on the subcell. Four orders of satellites are shown; the size of the circles in the figure decrease with increasing order.

Based on the large side face-centred monoclinic cell, more than 14000 reflections were collected at room temperature in ω–2θ scan mode. An analytical absorption correction was made using *LSABS* (Blanc, Schwarzenbach & Flack, 1991), the anomalous dispersion coefficients were taken from the *International Tables for X-ray Crystallography* (1974, Vol. IV). A preliminary refinement was performed in the orthorhombic subcell in space group *Ccc*2 down to $wR = 0.026$. The superstructure was refined in the large monoclinic cell by the least-squares method based on $|F|$ values, starting from positions derived from rocksalt- and perovskite-type atom arrangements. Details of the structure refinements are compared in Table 3. Owing to the difficulties in determining the O-atom positions in the superstructure, the isotropic displacement parameters of the O sites were fixed at 0.02 $Å^2$. After a few cycles two additional O sites were tested and then retained in all further refinements. 579 parameters (a scale factor, isotropic extinction, atomic positional, displacement and population parameters) were progressively refined on all 7227 unique reflections down to $wR = 0.057$.

The programs used for the data reduction and structure refinements are all from the *Xtal*3.2 system (Hall, Flack & Stewart, 1992). The atomic positional (equivalent), isotropic displacement and population parameters of the average structure are given in Table 4 and the anisotropic displacement parameters of the cation sites from the same refinement in Table 5. The atomic positional, (equivalent) isotropic displacement and population parameters of the superstructure are listed in Table 6 and selected interatomic distances in Table 7.*

3. Results and discussion

3.1. *Average structure*

The idealized structure of $Bi_2Sr_2CaCu_2O_{8+\delta}$ may be considered as built up of two types of slabs: a rocksalt-derived slab containing two BiO layers and a perovskite-derived SrO–CuO_2–Ca–CuO_2–SrO slab. The atomic coordinates of the average structure, listed in Table 4, were refined in non-centrosymmetric space group *Ccc*2, where **a** is the short translation vector, **b** is perpendicular to the atom layers (stacking direction) and **c** is parallel to the modulation direction. The Bi site was split into two positions, the distance between the two partly (55 and 45%) occupied sites being 0.59 Å. In agreement with literature data, which all show the formation of Bi zigzag chains parallel to one of the short translation vectors, the x coordinate of the Bi sites differs significantly from 1/4. The deformations of the BiO layers from the ideal rocksalt-type atom arrangement have allowed the Bi atoms to decrease the number of nearest O neighbours from six to three. The excess Bi was found on the Ca site (10% substitution) and 11% Ca was located on the Sr site, giving the composition $Bi_{2.10}Sr_{1.78}Ca_{1.12}Cu_2O_8$. The displacive modulation is reflected in the high values of the atomic displacement parameters. The anisotropic displacement parameters of the metal atom sites are listed in Table 5 and their ellipsoid representations are shown in Fig. 2 in a projection along [100]. It can be seen that the ellipsoids of the Bi and Sr sites have large components both along [010] and [001], whereas those of the Cu and Ca sites are elongated along [010]. The

* A list of structure factors has been deposited with the IUCr (Reference: DU0400). Copies may be obtained through The Managing Editor, International Union of Crystallography, 5 Abbey Square, Chester CH1 2HU, England.

Table 6. *Fractional atomic coordinates, isotropic or equivalent displacement parameters ($Å^2 \times 10^2$) and population parameters in the superstructure of $Bi_{2.09(2)}Sr_{1.90(2)}Ca_{1.00(4)}Cu_2O_{8.22}$, space group Cc*

All atoms sites are in Wyckoff position 4(*a*). The displacement parameters were refined anisotropically for the Bi sites, isotropically for all other metal atom sites; U_{iso} was fixed to 0.02 $Å^2$ for the O sites. E.s.d.'s are less than 7 on the last digit of the positional and displacement parameters of the metal-atom sites, less than 3 for the coordinates of the O sites. Letters *A* and *B* in the site labels refer to the crystallographically independent layers marked in Fig. 3; the sites are numbered from left to right within the asymmetric unit delimited by dashed lines in the same figure.

$$U_{eq} = (1/3)\sum_i \sum_j U_{ij} a_i^* a_j^* \mathbf{a}_i \cdot \mathbf{a}_j.$$

	x	*y*	*z*	$U_{iso/eq}$	Ca/Bi†
Bi(1*A*)	0.9759	0.530	0.0199	7.8‡	
Bi(2*A*)	0.0385	0.966	0.0824	5.1	
Bi(3*A*)	0.0949	0.519	0.1424	2.4	
Bi(4*A*)	0.1461	0.963	0.1968	1.4	
Bi(5*A*)	0.1963	0.521	0.2495	2.4	
Bi(6*A*)	0.2491	0.990	0.3013	1.8	
Bi(7*A*)	0.3011	0.511	0.3527	2.2	
Bi(8*A*)	0.3542	0.979	0.4032	3.2	
Bi(9*A*)	0.4169	0.538	0.4611	5.6	
Sr(1*A*)	0.9266	0.001	0.0564	3.3§	
Sr(2*A*)	0.9892	0.499	0.1186	2.7	
Sr(3*A*)	0.0434	0.998	0.1795	4.8	
Sr(4*A*)	0.0943	0.491	0.2330	0.8	
Sr(5*A*)	0.1473	0.999	0.2865	0.9	
Sr(6*A*)	0.1963	0.495	0.3433	0.7	
Sr(7*A*)	0.2531	0.002	0.3952	0.8	
Sr(8*A*)	0.3056	0.499	0.4500	0.9	
Sr(9*A*)	0.3658	0.000	0.4986	1.5	
Cu(1*A*)	0.8990	0.501	0.0845	3.9	
Cu(2*A*)	0.9537	0.000	0.1385	1.4	
Cu(3*A*)	0.0077	0.495	0.1983	0.7	
Cu(4*A*)	0.0588	0.993	0.2584	0.8	
Cu(5*A*)	0.1111	0.499	0.3150	0.6	
Cu(6*A*)	0.1675	0.991	0.3697	0.8	
Cu(7*A*)	0.2211	0.494	0.4236	0.9	
Cu(8*A*)	0.2796	0.004	0.4751	0.8	
Cu(9*A*)	0.3438	0.502	0.5278	0.8	
Bi(1*B*)	0.7589	0.465	0.1972	1.2	
Bi(2*B*)	0.8103	0.019	0.2495	2.4	
Bi(3*B*)	0.8606	0.478	0.3041	2.8	
Bi(4*B*)	0.9127	0.005	0.3595	2.9	
Bi(5*B*)	0.9718	0.470	0.4216	6.9	
Bi(6*B*)	0.0336	0.029	0.4814	6.6¶	
Bi(7*B*)	0.0958	0.477	0.5418	3.9	
Bi(8*B*)	0.1513	0.029	0.5953	1.8	
Bi(9*B*)	0.2062	0.484	0.6470	1.7	
Sr(1*B*)	0.8071	0.994	0.1569	2.0	
Sr(2*B*)	0.8625	0.500	0.2098	1.0	
Sr(3*B*)	0.9141	0.999	0.2657	0.8	
Sr(4*B*)	0.9633	0.500	0.3242	1.5	
Sr(5*B*)	0.0172	0.998	0.3806	1.0	
Sr(6*B*)	0.0798	0.499	0.4435	3.2**	
Sr(7*B*)	0.1376	0.001	0.4996	1.3	
Sr(8*B*)	0.1957	0.508	0.5545	3.3	
Sr(9*B*)	0.2510	0.004	0.6070	1.0	
Cu(1*B*)	0.8386	0.498	0.1346	1.4	
Cu(2*B*)	0.8933	0.994	0.1872	1.0	
Cu(3*B*)	0.9467	0.494	0.2413	0.8	
Cu(4*B*)	0.9983	0.995	0.3023	0.9	
Cu(5*B*)	0.0515	0.495	0.3583	1.1	
Cu(6*B*)	0.1053	0.996	0.4188	0.9	
Cu(7*B*)	0.1699	0.498	0.4717	1.1	
Cu(8*B*)	0.2234	0.004	0.5253	1.7	
Cu(9*B*)	0.2821	0.504	0.5781	1.5	
Ca(1)	0.8707	0.999	0.1056	1.1	0.91/0.09
Ca(2)	0.9242	0.506	0.1634	1.5	0.95/0.05
Ca(3)	0.9775	0.000	0.2227	1.7	0.91/0.09
Ca(4)	0.0310	0.505	0.2810	2.4	0.85/0.15
Ca(5)	0.0829	0.010	0.3354	2.6	0.90/0.10
Ca(6)	0.1362	0.498	0.3916	1.0	0.86/0.14
Ca(7)	0.1964	0.004	0.4454	1.4	0.92/0.08
Ca(8)	0.2482	0.509	0.5003	1.0	0.92/0.08
Ca(9)	0.3122	0.000	0.5519	1.9	0.91/0.09

Table 6 (*cont.*)

	x	*y*	*z*	$U_{iso/eq}$	Ca/Bi†
O(1*A*)	0.989	0.83	0.056		
O(2*A*)	0.044	0.82	0.123		
O(3*A*)	0.094	0.95	0.150		
O(4*A*)	0.138	0.52	0.200		
O(5*A*)	0.205	0.90	0.255		
O(6*A*)	0.245	0.61	0.297		
O(7*A*)	0.297	0.92	0.351		
O(8*A*)	0.337	0.63	0.406		
O(9*A*)	0.375	0.86	0.450		
O(10*A*)	0.439	0.63	0.504		
O(11*A*)	0.949	0.46	0.070		
O(12*A*)	0.986	0.01	0.100		
O(13*A*)	0.060	0.51	0.168		
O(14*A*)	0.109	0.97	0.229		
O(15*A*)	0.163	0.44	0.278		
O(16*A*)	0.213	0.02	0.330		
O(17*A*)	0.265	0.44	0.382		
O(18*A*)	0.319	0.02	0.433		
O(19*A*)	0.382	0.50	0.492		
O(20*A*)	0.928	0.24	0.113		
O(21*A*)	0.935	0.73	0.104		
O(22*A*)	0.983	0.25	0.170		
O(23*A*)	0.985	0.75	0.168		
O(24*A*)	0.031	0.24	0.231		
O(25*A*)	0.022	0.75	0.237		
O(26*A*)	0.087	0.23	0.285		
O(27*A*)	0.081	0.73	0.287		
O(28*A*)	0.136	0.24	0.343		
O(29*A*)	0.144	0.75	0.339		
O(30*A*)	0.199	0.25	0.394		
O(31*A*)	0.190	0.74	0.397		
O(32*A*)	0.249	0.22	0.449		
O(33*A*)	0.255	0.72	0.446		
O(34*A*)	0.310	0.24	0.502		
O(35*A*)	0.311	0.79	0.501		
O(36*A*)	0.376	0.28	0.555		
O(37*A*)	0.368	0.77	0.559		
O(1*B*)	0.741	0.01	0.196		
O(2*B*)	0.811	0.49	0.255		
O(3*B*)	0.861	0.05	0.296		
O(4*B*)	0.903	0.41	0.351		
O(5*B*)	0.949	0.10	0.399		
O(6*B*)	0.010	0.37	0.455		
O(7*B*)	0.055	0.40	0.502		
O(8*B*)	0.110	0.09	0.555		
O(9*B*)	0.162	0.40	0.602		
O(10*B*)	0.199	0.02	0.636		
O(11*B*)	0.789	0.52	0.169		
O(12*B*)	0.846	0.97	0.221		
O(13*B*)	0.894	0.52	0.278		
O(14*B*)	0.951	0.98	0.333		
O(15*B*)	0.006	0.54	0.379		
O(16*B*)	0.079	0.09	0.473		
O(17*B*)	0.136	0.54	0.518		
O(18*B*)	0.187	0.99	0.565		
O(19*B*)	0.242	0.54	0.617		
O(20*B*)	0.869	0.24	0.158		
O(21*B*)	0.868	0.73	0.158		
O(22*B*)	0.917	0.24	0.217		
O(23*B*)	0.926	0.76	0.210		
O(24*B*)	0.976	0.26	0.269		
O(25*B*)	0.970	0.75	0.277		
O(26*B*)	0.022	0.24	0.335		
O(27*B*)	0.030	0.74	0.328		
O(28*B*)	0.084	0.24	0.389		
O(29*B*)	0.079	0.74	0.390		
O(30*B*)	0.133	0.25	0.447		
O(31*B*)	0.147	0.80	0.443		
O(32*B*)	0.202	0.26	0.495		
O(33*B*)	0.189	0.74	0.502		
O(34*B*)	0.260	0.25	0.548		
O(35*B*)	0.255	0.75	0.551		
O(36*B*)	0.312	0.26	0.604		
O(37*B*)	0.320	0.75	0.597		

† E.s.d. = 0.02. ‡ *PP* = 0.96 (2). § 0.75 (8) Sr + 0.25 (8) Ca. ¶ *PP* = 0.94 (2). ** 0.37 (8) Sr + 0.63 (8) Ca.

Table 7. *Interatomic distances (Å) in* $Bi_{2.09}Sr_{1.90}Ca_{1.00}Cu_2O_{8.22}$, *space group Cc*

Bi—O distances are listed up to 3.7 Å, Sr—O distances up to 3.5 Å, Cu—O and Ca—O distances up to 3 Å. E.s.d.'s are less than 12 on the last digit. O sites numbered from 1 to 10 belong to the BiO layers, sites from 11 to 19 to the SrO layers and sites from 20 to 37 to the CuO_2 layers.

Bi(1A)—O(1A)	2.17	Bi(4A)—O(14A)	2.16	Bi(7A)—O(17A)	2.07
Bi(1A)—O(10A)	2.30	Bi(4A)—O(3A)	2.41	Bi(7A)—O(7A)	2.23
Bi(1A)—O(11A)	2.51	Bi(4A)—O(4A)	2.42	Bi(7A)—O(8A)	2.39
Bi(1A)—O(7B)	3.26	Bi(4A)—O(5A)	2.88	Bi(7A)—O(6A)	2.78
Bi(1A)—O(6B)	3.26	Bi(4A)—O(4A)	3.05	Bi(7A)—O(7A)	3.19
		Bi(4A)—O(10B)	3.54	Bi(7A)—O(3B)	3.62
Bi(2A)—O(2A)	1.81	Bi(5A)—O(15A)	1.95	Bi(8A)—O(9A)	1.99
Bi(2A)—O(1A)	2.05	Bi(5A)—O(5A)	2.07	Bi(8A)—O(8A)	2.01
Bi(2A)—O(12A)	2.27	Bi(5A)—O(6A)	2.39	Bi(8A)—O(18A)	2.02
Bi(2A)—O(3A)	3.06	Bi(5A)—O(4A)	2.62	Bi(8A)—O(7A)	2.68
Bi(2A)—O(8B)	3.17	Bi(5A)—O(1B)	3.10	Bi(8A)—O(4B)	3.17
		Bi(5A)—O(5A)	3.39	Bi(8A)—O(8A)	3.59
Bi(3A)—O(13A)	1.86	Bi(6A)—O(16A)	2.01	Bi(9A)—O(10A)	1.83
Bi(3A)—O(3A)	2.33	Bi(6A)—O(6A)	2.07	Bi(9A)—O(19A)	2.06
Bi(3A)—O(2A)	2.48	Bi(6A)—O(5A)	2.27	Bi(9A)—O(9A)	2.34
Bi(3A)—O(4A)	2.55	Bi(6A)—O(7A)	2.42	Bi(9A)—O(5B)	3.08
Bi(3A)—O(3A)	3.12	Bi(6A)—O(2B)	3.35	Bi(9A)—O(8A)	3.35
Bi(3A)—O(9B)	3.38	Bi(6A)—O(6A)	3.36		
Sr(1A)—O(36A)	2.21	Sr(4A)—O(4A)	2.36	Sr(7A)—O(30A)	2.44
Sr(1A)—O(21A)	2.39	Sr(4A)—O(26A)	2.64	Sr(7A)—O(17A)	2.47
Sr(1A)—O(10A)	2.42	Sr(4A)—O(13A)	2.68	Sr(7A)—O(32A)	2.53
Sr(1A)—O(12A)	2.52	Sr(4A)—O(14A)	2.68	Sr(7A)—O(33A)	2.57
Sr(1A)—O(1A)	2.55	Sr(4A)—O(27A)	2.70	Sr(7A)—O(18A)	2.59
Sr(1A)—O(20A)	2.65	Sr(4A)—O(24A)	2.74	Sr(7A)—O(16A)	2.75
Sr(1A)—O(11A)	2.65	Sr(4A)—O(15A)	2.81	Sr(7A)—O(7A)	2.77
Sr(1A)—O(37A)	2.67	Sr(4A)—O(14A)	2.86	Sr(7A)—O(31A)	2.79
Sr(1A)—O(19A)	2.79	Sr(4A)—O(25A)	3.11	Sr(7A)—O(17A)	3.16
Sr(1A)—O(11A)	3.04				
Sr(2A)—O(11A)	2.23	Sr(5A)—O(14A)	2.45	Sr(8A)—O(33A)	2.20
Sr(2A)—O(21A)	2.33	Sr(5A)—O(15A)	2.51	Sr(8A)—O(8A)	2.47
Sr(2A)—O(23A)	2.48	Sr(5A)—O(29A)	2.57	Sr(8A)—O(34A)	2.54
Sr(2A)—O(22A)	2.56	Sr(5A)—O(26A)	2.57	Sr(8A)—O(35A)	2.58
Sr(2A)—O(2A)	2.68	Sr(5A)—O(16A)	2.70	Sr(8A)—O(32A)	2.59
Sr(2A)—O(20A)	2.68	Sr(5A)—O(28A)	2.78	Sr(8A)—O(18A)	2.76
Sr(2A)—O(12A)	2.76	Sr(5A)—O(5A)	2.86	Sr(8A)—O(17A)	2.87
Sr(2A)—O(12A)	2.85	Sr(5A)—O(27A)	2.90	Sr(8A)—O(18A)	2.98
Sr(2A)—O(13A)	2.96	Sr(5A)—O(15A)	3.11	Sr(8A)—O(19A)	2.98
Sr(2A)—O(1A)	3.11			Sr(8A)—O(9A)	3.27
Sr(3A)—O(3A)	2.52	Sr(6A)—O(29A)	2.39	Sr(9A)—O(9A)	2.24
Sr(3A)—O(23A)	2.52	Sr(6A)—O(30A)	2.45	Sr(9A)—O(35A)	2.39
Sr(3A)—O(2A)	2.54	Sr(6A)—O(31A)	2.63	Sr(9A)—O(34A)	2.50
Sr(3A)—O(24A)	2.61	Sr(6A)—O(28A)	2.66	Sr(9A)—O(36A)	2.72
Sr(3A)—O(22A)	2.62	Sr(6A)—O(16A)	2.71	Sr(9A)—O(37A)	2.76
Sr(3A)—O(13A)	2.80	Sr(6A)—O(15A)	2.71	Sr(9A)—O(19A)	2.77
Sr(3A)—O(14A)	2.82	Sr(6A)—O(17A)	2.72	Sr(9A)—O(19A)	2.82
Sr(3A)—O(13A)	2.89	Sr(6A)—O(16A)	3.00	Sr(9A)—O(18A)	2.88
Sr(3A)—O(25A)	2.98	Sr(6A)—O(6A)	3.01	Sr(9A)—O(10A)	3.37
Sr(3A)—O(12A)	3.47				
Cu(1A)—O(37A)	1.87	Cu(4A)—O(26A)	1.84	Cu(7A)—O(30A)	1.84
Cu(1A)—O(21A)	1.88	Cu(4A)—O(24A)	1.89	Cu(7A)—O(33A)	1.84
Cu(1A)—O(20A)	1.99	Cu(4A)—O(27A)	1.93	Cu(7A)—O(31A)	1.95
Cu(1A)—O(36A)	2.03	Cu(4A)—O(25A)	1.98	Cu(7A)—O(32A)	1.97
Cu(1A)—O(11A)	2.12	Cu(4A)—O(14A)	2.46	Cu(7A)—O(17A)	2.66
Cu(2A)—O(20A)	1.80	Cu(5A)—O(27A)	1.87	Cu(8A)—O(32A)	1.81
Cu(2A)—O(22A)	2.01	Cu(5A)—O(28A)	1.90	Cu(8A)—O(35A)	1.84
Cu(2A)—O(23A)	2.01	Cu(5A)—O(29A)	1.97	Cu(8A)—O(34A)	1.90
Cu(2A)—O(21A)	2.06	Cu(5A)—O(26A)	2.00	Cu(8A)—O(33A)	2.05
Cu(2A)—O(12A)	2.21	Cu(5A)—O(15A)	2.77	Cu(8A)—O(18A)	2.54
Cu(3A)—O(22A)	1.87	Cu(6A)—O(31A)	1.82	Cu(9A)—O(36A)	1.87
Cu(3A)—O(23A)	1.91	Cu(6A)—O(29A)	1.86	Cu(9A)—O(37A)	1.98
Cu(3A)—O(24A)	1.99	Cu(6A)—O(28A)	1.97	Cu(9A)—O(34A)	2.03
Cu(3A)—O(25A)	2.06	Cu(6A)—O(30A)	1.97	Cu(9A)—O(35A)	2.10
Cu(3A)—O(13A)	2.58	Cu(6A)—O(16A)	2.63	Cu(9A)—O(19A)	2.27
Bi(1B)—O(11B)	1.85	Bi(2B)—O(12B)	1.99	Bi(3B)—O(13B)	1.87
Bi(1B)—O(1B)	2.54	Bi(2B)—O(3B)	2.38	Bi(3B)—O(4B)	2.22
Bi(1B)—O(2B)	2.70	Bi(2B)—O(2B)	2.54	Bi(3B)—O(3B)	2.34
Bi(1B)—O(10B)	2.97	Bi(2B)—O(2B)	2.89	Bi(3B)—O(2B)	2.41
Bi(1B)—O(1B)	3.02	Bi(2B)—O(1B)	3.00	Bi(3B)—O(3B)	3.11
Bi(1B)—O(5A)	3.47	Bi(2B)—O(6A)	3.52	Bi(3B)—O(7A)	3.42

Table 7 (*cont.*)

Bi(4B)—O(5B)	1.94	Bi(6B)—O(16B)	1.84	Bi(8B)—O(8B)	2.01
Bi(4B)—O(14B)	2.00	Bi(6B)—O(6B)	2.20	Bi(8B)—O(18B)	2.06
Bi(4B)—O(4B)	2.23	Bi(6B)—O(7B)	2.25	Bi(8B)—O(9B)	2.07
Bi(4B)—O(3B)	2.87	Bi(6B)—O(7B)	3.56	Bi(8B)—O(10B)	2.14
Bi(4B)—O(4B)	3.26	Bi(6B)—O(8B)	3.68	Bi(8B)—O(9B)	3.41
				Bi(8B)—O(3A)	3.46
Bi(5B)—O(6B)	1.83	Bi(7B)—O(7B)	2.00	Bi(9B)—O(19B)	2.07
Bi(5B)—O(5B)	2.27	Bi(7B)—O(17B)	2.03	Bi(9B)—O(1B)	2.12
Bi(5B)—O(15B)	2.45	Bi(7B)—O(8B)	2.18	Bi(9B)—O(9B)	2.23
Bi(5B)—O(4B)	3.43	Bi(7B)—O(9B)	3.10	Bi(9B)—O(10B)	2.55
Bi(5B)—O(5B)	3.60	Bi(7B)—O(8B)	3.40	Bi(9B)—O(10B)	2.94
		Bi(7B)—O(16B)	3.46		
Sr(1B)—O(36B)	2.57	Sr(4B)—O(25B)	2.41	Sr(7B)—O(16B)	2.29
Sr(1B)—O(19B)	2.62	Sr(4B)—O(15B)	2.43	Sr(7B)—O(33B)	2.38
Sr(1B)—O(20B)	2.68	Sr(4B)—O(26B)	2.57	Sr(7B)—O(30B)	2.50
Sr(1B)—O(21B)	2.69	Sr(4B)—O(14B)	2.67	Sr(7B)—O(17B)	2.58
Sr(1B)—O(11B)	2.70	Sr(4B)—O(24B)	2.76	Sr(7B)—O(31B)	2.69
Sr(1B)—O(12B)	2.70	Sr(4B)—O(4B)	2.78	Sr(7B)—O(8B)	2.77
Sr(1B)—O(37B)	2.91	Sr(4B)—O(27B)	2.82	Sr(7B)—O(32B)	2.85
Sr(1B)—O(11B)	3.01	Sr(4B)—O(13B)	2.84	Sr(7B)—O(18B)	2.87
Sr(1B)—O(1B)	3.25	Sr(4B)—O(14B)	2.90	Sr(7B)—O(17B)	3.04
Sr(2B)—O(22B)	2.44	Sr(5B)—O(26B)	2.35	Sr(8B)—O(17B)	2.42
Sr(2B)—O(21B)	2.50	Sr(5B)—O(15B)	2.52	Sr(8B)—O(33B)	2.45
Sr(2B)—O(20B)	2.60	Sr(5B)—O(29B)	2.67	Sr(8B)—O(9B)	2.62
Sr(2B)—O(12B)	2.70	Sr(5B)—O(27B)	2.68	Sr(8B)—O(35B)	2.62
Sr(2B)—O(23B)	2.77	Sr(5B)—O(28B)	2.77	Sr(8B)—O(18B)	2.67
Sr(2B)—O(13B)	2.77	Sr(5B)—O(14B)	2.80	Sr(8B)—O(19B)	2.75
Sr(2B)—O(11B)	2.88	Sr(5B)—O(5B)	2.92	Sr(8B)—O(32B)	2.83
Sr(2B)—O(2B)	2.98	Sr(5B)—O(15B)	2.95	Sr(8B)—O(18B)	2.87
Sr(2B)—O(12B)	2.98			Sr(8B)—O(34B)	2.87
Sr(3B)—O(22B)	2.40	Sr(6B)—O(30B)	2.39	Sr(9B)—O(10B)	2.53
Sr(3B)—O(25B)	2.45	Sr(6B)—O(29B)	2.53	Sr(9B)—O(19B)	2.55
Sr(3B)—O(3B)	2.60	Sr(6B)—O(16B)	2.55	Sr(9B)—O(11B)	2.61
Sr(3B)—O(24B)	2.71	Sr(6B)—O(28B)	2.68	Sr(9B)—O(18B)	2.63
Sr(3B)—O(13B)	2.75	Sr(6B)—O(7B)	2.84	Sr(9B)—O(35B)	2.71
Sr(3B)—O(23B)	2.77	Sr(6B)—O(6B)	2.88	Sr(9B)—O(36B)	2.72
Sr(3B)—O(12B)	2.79	Sr(6B)—O(31B)	3.03	Sr(9B)—O(34B)	2.86
Sr(3B)—O(14B)	2.79	Sr(6B)—O(17B)	3.28	Sr(9B)—O(19B)	2.98
Sr(3B)—O(13B)	3.01	Sr(6B)—O(15B)	3.38	Sr(9B)—O(37B)	3.07
		Sr(6B)—O(16B)	3.41		
Cu(1B)—O(21B)	1.81	Cu(4B)—O(25B)	1.89	Cu(7B)—O(33B)	1.82
Cu(1B)—O(20B)	1.90	Cu(4B)—O(27B)	1.96	Cu(7B)—O(32B)	1.87
Cu(1B)—O(36B)	1.99	Cu(4B)—O(26B)	1.96	Cu(7B)—O(30B)	2.04
Cu(1B)—O(37B)	2.06	Cu(4B)—O(24B)	2.03	Cu(7B)—O(31B)	2.08
Cu(1B)—O(11B)	2.58	Cu(4B)—O(14B)	2.43	Cu(7B)—O(17B)	2.53
Cu(2B)—O(23B)	1.85	Cu(5B)—O(26B)	1.87	Cu(8B)—O(32B)	1.91
Cu(2B)—O(22B)	1.89	Cu(5B)—O(27B)	1.87	Cu(8B)—O(35B)	1.94
Cu(2B)—O(20B)	1.89	Cu(5B)—O(29B)	1.97	Cu(8B)—O(34B)	2.00
Cu(2B)—O(21B)	1.95	Cu(5B)—O(28B)	2.07	Cu(8B)—O(33B)	2.03
Cu(2B)—O(12B)	2.51	Cu(5B)—O(15B)	2.09	Cu(8B)—O(18B)	2.36
Cu(3B)—O(24B)	1.88	Cu(6B)—O(28B)	1.84	Cu(9B)—O(36B)	1.89
Cu(3B)—O(22B)	1.90	Cu(6B)—O(30B)	1.93	Cu(9B)—O(34B)	1.89
Cu(3B)—O(23B)	1.98	Cu(6B)—O(29B)	1.94	Cu(9B)—O(35B)	1.90
Cu(3B)—O(25B)	2.03	Cu(6B)—O(31B)	1.97	Cu(9B)—O(37B)	1.97
Cu(3B)—O(13B)	2.75	Cu(6B)—O(16B)	2.70	Cu(9B)—O(19B)	2.44
Ca(1)—O(37B)	2.28	Ca(3)—O(25A)	2.12	Ca(5)—O(28A)	2.32
Ca(1)—O(37A)	2.38	Ca(3)—O(23B)	2.31	Ca(5)—O(26A)	2.41
Ca(1)—O(36A)	2.45	Ca(3)—O(24A)	2.35	Ca(5)—O(27B)	2.42
Ca(1)—O(20A)	2.47	Ca(3)—O(24B)	2.37	Ca(5)—O(27A)	2.50
Ca(1)—O(20B)	2.54	Ca(3)—O(22A)	2.60	Ca(5)—O(28B)	2.52
Ca(1)—O(36B)	2.55	Ca(3)—O(22B)	2.61	Ca(5)—O(26B)	2.61
Ca(1)—O(21B)	2.63	Ca(3)—O(23A)	2.69	Ca(5)—O(29A)	2.67
Ca(1)—O(21A)	2.87	Ca(3)—O(25B)	2.70	Ca(5)—O(29B)	2.73
Ca(2)—O(23B)	2.33	Ca(4)—O(27A)	2.21	Ca(6)—O(31A)	2.38
Ca(2)—O(21B)	2.41	Ca(4)—O(25A)	2.21	Ca(6)—O(28B)	2.42
Ca(2)—O(20B)	2.50	Ca(4)—O(27B)	2.35	Ca(6)—O(28A)	2.44
Ca(2)—O(20A)	2.55	Ca(4)—O(24B)	2.41	Ca(6)—O(29B)	2.52
Ca(2)—O(22A)	2.57	Ca(4)—O(24A)	2.52	Ca(6)—O(31B)	2.60
Ca(2)—O(23A)	2.62	Ca(4)—O(26A)	2.58	Ca(6)—O(29A)	2.63
Ca(2)—O(22B)	2.71	Ca(4)—O(25B)	2.63	Ca(6)—O(30B)	2.69
Ca(2)—O(21A)	2.85	Ca(4)—O(26B)	2.71	Ca(6)—O(30A)	2.70

Table 7 (*cont.*)

Ca(7)—O(31*B*)	2.14	Ca(8)—O(32*B*)	2.17	Ca(9)—O(37*B*)	2.27
Ca(7)—O(32*A*)	2.29	Ca(8)—O(34*B*)	2.36	Ca(9)—O(34*B*)	2.36
Ca(7)—O(31*A*)	2.41	Ca(8)—O(35*B*)	2.42	Ca(9)—O(35*A*)	2.37
Ca(7)—O(32*B*)	2.45	Ca(8)—O(33*B*)	2.58	Ca(9)—O(34*A*)	2.41
Ca(7)—O(30*A*)	2.52	Ca(8)—O(33*A*)	2.58	Ca(9)—O(37*A*)	2.41
Ca(7)—O(33*A*)	2.71	Ca(8)—O(32*A*)	2.65	Ca(9)—O(35*B*)	2.55
Ca(7)—O(30*B*)	2.77	Ca(8)—O(34*A*)	2.75	Ca(9)—O(36*B*)	2.59
Ca(7)—O(33*B*)	2.81	Ca(8)—O(35*A*)	2.80	Ca(9)—O(36*A*)	2.85

highest displacement parameters are observed for the oxygen sites in the BiO and SrO layers [O(1) and O(2), respectively].

3.2. *Superstructure*

Fig. 3 shows the structure of the title compound in a projection along [010], referring to the monoclinic supercell. The supercell, which is indicated with dotted lines on the drawing, can be obtained from the orthorhombic cell of the average structure, indicated with solid lines, by applying the following transformation

$$\mathbf{a}_m = \mathbf{b}_o + 4\mathbf{c}_o,\ \mathbf{b}_m = -\mathbf{a}_o,\ \mathbf{c}_m = -\mathbf{b}_o + 5\mathbf{c}_o.$$

The (main) cation of each atom layer is indicated on the right-hand side of the projection. It clearly appears that all layers suffer a displacive modulation, with the modulation wavevector along the diagonal [101] of the monoclinic supercell.

The compounds of the $Bi_2Sr_2Ca_{n-1}Cu_nO_{4+2n+\delta}$ structure series have a strong two-dimensional character with a cleavage plane between the two BiO layers. An alternative way to describe the structures is to consider it as being built up of one type of structural slab, delimited by a BiO layer on each side. The strongest covalent bonding is to be found between Cu and O and between Bi and O atoms, and this can be expected to determine the main geometrical features. The Cu atoms are located near the base of elongated square pyramids formed by five O atoms, the sixth atom of a true perovskite-type atom arrangement being absent. The square-mesh CuO_2 nets are relatively rigid in comparison to the BiO layers which undergo strong distortions with respect to the ideal rocksalt-type atom arrangement and are able to accommodate different amounts of additional O atoms. The Bi and Cu atoms are interconnected *via* the apical O atoms of the square pyramids, situated in the SrO layers.

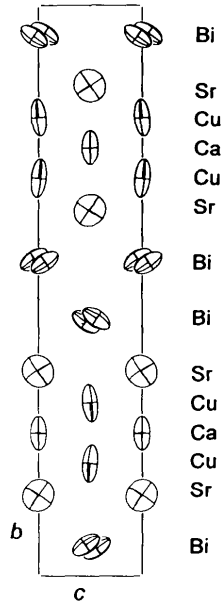

Fig. 2. A section of the average structure of $Bi_2Sr_2CaCu_2O_{8+\delta}$, space group *Ccc*2, in a projection along [100]. Only the displacement ellipsoids of the metal atom sites at $x \approx 1/4$ (99% probability level) are shown.

3.3. *Metal-atom waves*

The displacements of the metal atoms, and in particular those of the Bi atoms, from the ideal positions of the rocksalt- and perovskite-type substructures, are complex. The component along the short translation vector [010] appears to be commensurate with the ideal structure and is, as shown above, already taken into consideration in the average structure on lowering its symmetry from tetragonal to orthorhombic. It can be seen from Table 6 that there are no significant shifts from the ideal values 0 and $\frac{1}{2}$ for the y coordinates of the Sr, Cu or Ca sites, however, the y coordinates of the Bi sites in layer *A* [Bi(1*A*)–Bi(9*A*)] are systematically closer to $\frac{3}{4}$, whereas the corresponding coordinates of the Bi sites in layer *B*[Bi(1*B*)–Bi(9*B*)] are closer to $\frac{1}{4}$. This confirms that the Bi atoms are arranged in zigzag chains inside the layers. The Bi—O—Cu—Cu—O—Bi segments, perpendicular to the atom layers, are tilted with respect to the (101) plane, *i.e.* the axes of the zigzag chains in one BiO layer are shifted by half the short translation unit with respect to the axes of the zigzag chains in the BiO layer on the other side of the same slab. This arrangement corresponds to the most frequent variant of orthorhombic $Bi_2Sr_2CaCu_2O_{8+\delta}$. A less common 'faulted structure' has been reported where the zigzag chains on both sides of the slab are not shifted with respect to each other in the direction of the short translation vector (Budin, Eibl, Pongratz & Skalicky, 1993). This type of stacking fault is easily recognized from HRTEM images perpendicular to the modulation vector where the dark spots corresponding to the metal atoms form large rectangles instead of the more common square-angle zigzag pattern. The average structure of the 'faulted structure' can be described in space group *Cmma* where **a** is parallel to the modulation direction, **b** to the stacking direction and **c** is the short translation vector.

Fig. 4 shows the best-fitting sinusoidal curves describing the displacements of the metal atom sites in the superstructure from ideal positions considering

rocksalt- and perovskite-type atom arrangements (*a*) perpendicular to the atom layers – transverse displacement – and (*b*) parallel to the modulation direction – longitudinal displacement. The open symbols represent the 7 × 9 metal-atom positions refined in the asymmetric unit delimited by dashed lines in Fig. 3. The Bi atoms of two additional layers have been considered (filled circles), one on each side of the complete slab, in

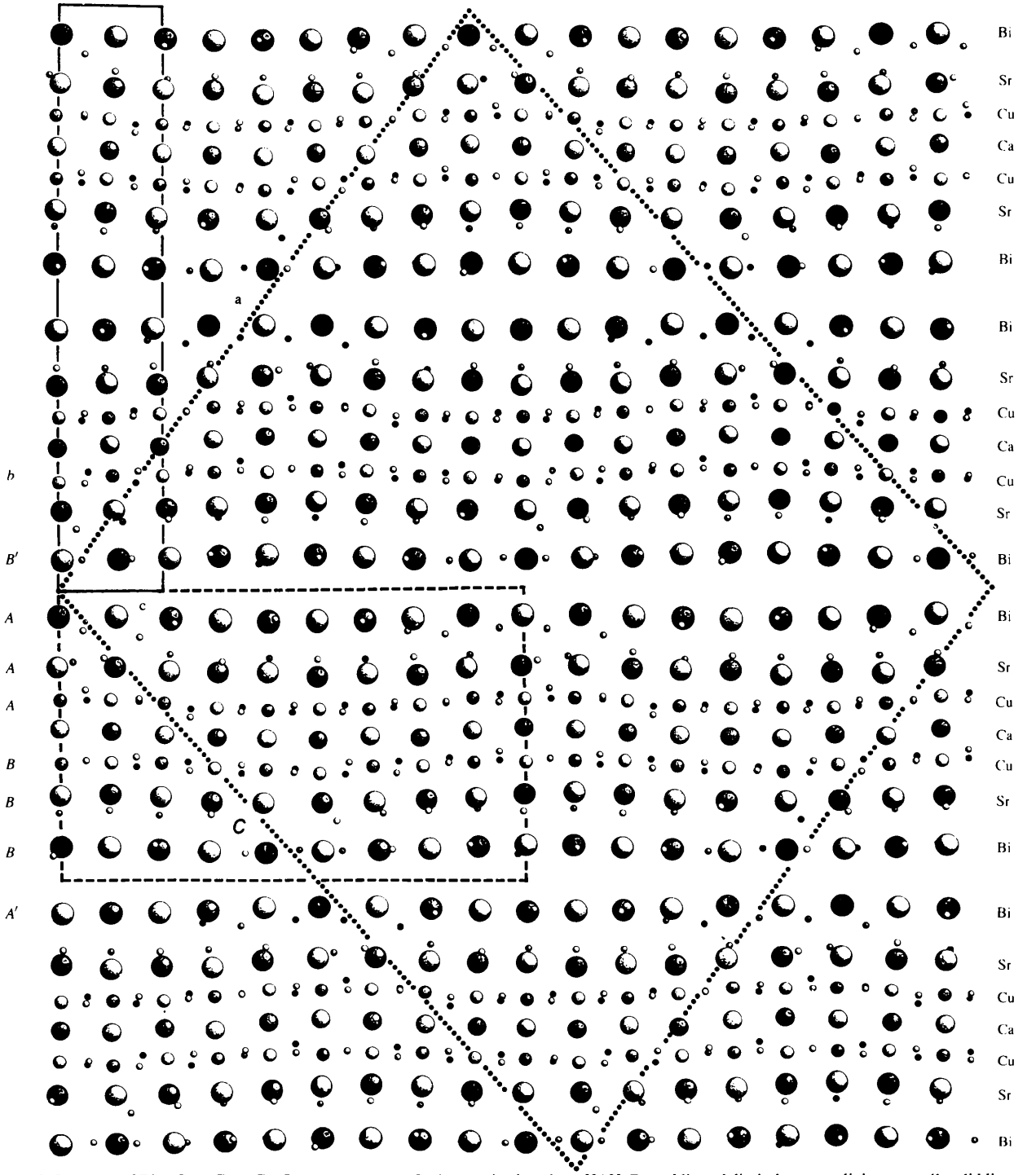

Fig. 3. Structure of $Bi_{2.09}Sr_{1.90}Ca_{1.00}Cu_2O_{8.22}$, space group *Cc*, in a projection along [010]. Dotted lines delimit the monoclinic supercell, solid lines the orthorhombic cell of the average structure. The (main) cation of each atom layer is indicated on the right-hand side of the drawing. Small circles represent O sites. The metal-atom sites in Table 6 are numbered from left to right within the asymmetric unit inside the rectangle drawn with dashed lines, letters *A* and *B* distinguished layers of the same composition.

order to show the wave sequence along the stacking direction. It can be seen that all atom sites are displaced perpendicular to the atom layers. The Bi atoms show in addition a high amplitude for the displacement along the modulation direction, which corresponds to the existence of Bi-rich and Bi-poor regions in the structure. For the Sr sites the amplitudes of the displacements perpendicular and parallel to the modulation direction are of similar magnitude. The Cu atoms show higher amplitude for the transverse than for the longitudinal displacement and the Ca sites have no significant displacement along the modulation direction.

The maxima and the minima of the sinusoidal curves describing the transverse displacements in Fig. 4 are indicated by arrows. As observed for the modulated structues of members of the $Bi_2Sr_2Ca_{n-1}Cu_nO_{4+2n+\delta}$ structure series reported in the literature, the displacements of the metal-atom sites are such that the waves of the transverse and longitudinal components show a phase difference of $\pi/2$. This means that the largest displacement parallel to the modulation vector is observed for a zero displacement in the perpendicular direction and *vice versa*. The combined transverse and longitudinal atom displacements observed for the metal-atom sites, and in particular the phase relations between the modulation waves, are in agreement with the model presented in Fig. 5, which is similar to the model proposed by Le Page, McKinnon, Tarascon & Barboux (1989). The thick slab shown in the central part of the figure represents the perovskite-derived structural slab delimited by a BiO layer on each side. In order to show the behaviour of the particular positions on the waves (zero, maximum and minimum amplitude), 12 points have been considered within the translation unit of the corrugation. It can be seen that when the slab is corrugated, only the points which are situated at the maxima and minima of the transverse displacement waves remain at their ideal positions with respect to the propagation direction. The points which are in an 'inner curve' of the corrugated slab are displaced towards each other, whereas those which are in an 'outer curve' move apart from each other. The points situated at the surface of the slab are projected on straight lines and the waves describing the displacements from the equidistant positions along the line are plotted in the upper and lower parts of the same figure. It can be seen that the largest longitudinal displacements correspond to a zero amplitude of the transverse displacement wave and that the longitudinal displacement waves show a phase shift of 90 (upper) and 270° (lower) with respect to the transverse displacement waves. The displacement of the points at the centre of the slab has no longitudinal component.

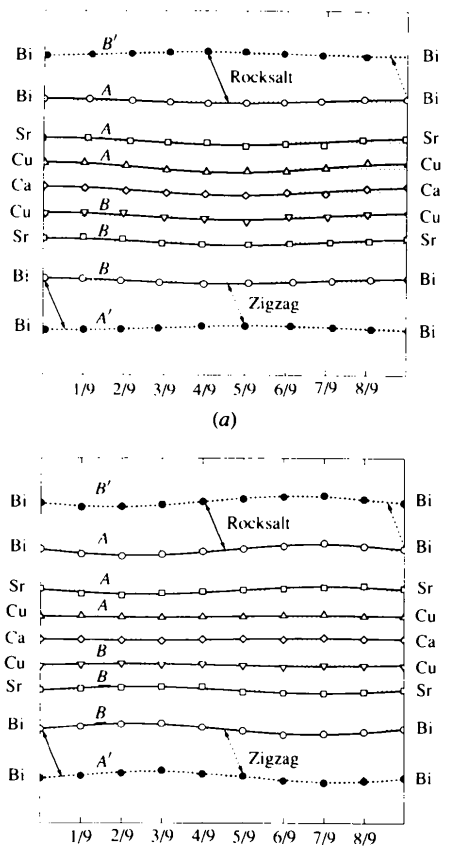

Fig. 4. Displacements of the metal-atom sites from ideal rocksalt and perovskite positions (*a*) perpendicular to the atom layers and (*b*) parallel to the modulation direction. Atom sites in the asymmetric unit indicated in Fig. 3 are represented by open symbols. Bi sites from the neighbouring BiO layers B' and A' by filled circles.

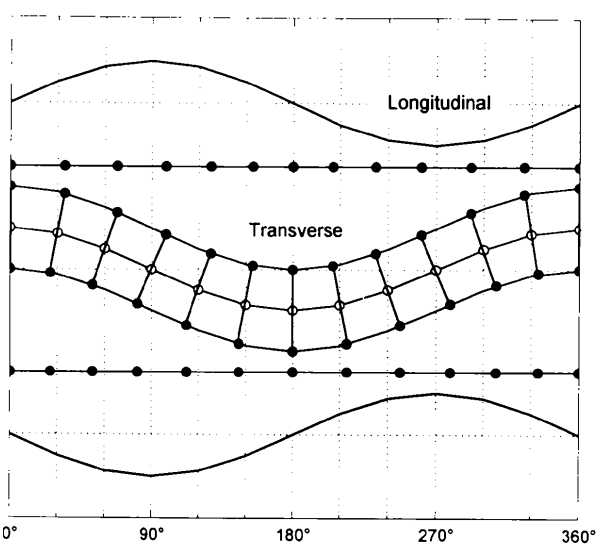

Fig. 5. Relationship between the transverse and longitudinal displacement waves of a corrugated slab, shown in the central part. The points situated on the surfaces of the slab are projected on straight lines. Note that 12 points were chosen for this model, whereas the structure reported here contains nine Bi-atom columns per translation unit of the modulation wave.

In the structure of $Bi_{10}Sr_{15}Fe_{10}O_{46}$, as well as in the commensurate models for orthorhombic $Bi_2Sr_2CaCu_2O_{8+\delta}$ which refer to a fivefold unit cell, the translation unit of the modulation wave corresponds to ten Bi-atom columns parallel to the short translation vector. In the monoclinic structure reported here, the translation unit of the modulation wave corresponds to nine Bi-atom columns, *i.e.* to an odd number of columns and the overall translation unit in the modulation direction ([101] vector of the monoclinic supercell) contains two complete waves. It can be seen from Fig. 4 that the maximum of the wave describing the transverse displacement of the Bi atoms in the layer labelled *A* coincides with a Bi-atom column [site Bi(1*A*)]. As a direct consequence of the odd number of atom columns in the translation unit of the modulation wave, the minimum of the same sinusoidal wave must go in between two Bi-atom columns [Bi(5*A*) and Bi(6*A*)]. The same is true for the wave describing the transverse displacement of the Bi atoms in layer *B*, which, as noted above, is in phase with the former. Two idealized slabs of similar characteristics are shown in Fig. 6 (it should be noted that the atoms in neighbouring columns of the real slabs are shifted by $\sim \mathbf{b}/2$ with respect to each other, *i.e.* perpendicular to the plane of the projection). One can imagine two ways to stack consecutive slabs so that Bi-poor (and Bi-rich) regions are superposed. Stacking with a mirror plane between the slabs would give two types of double BiO layers, one where the maxima and minima of the waves come close to each other at a Bi-atom column and one where they 'meet' between two Bi-atom columns. The second solution implies a relative translation of consecutive slabs by half the translation unit of the wave. A shift by exactly π is not, however, possible for an odd number of Bi-atom columns in the translation unit of the modulation wave, since this would correspond to a zigzag pattern of Bi-atom columns. An additional shift of $\pi/9 \equiv 20°$ is enough to respect the overall structural features. A systematic shift of consecutive slabs by $10\pi/9$ in the same direction leads to the monoclinic cell observed here. An alternative shift of consecutive slabs in opposite senses would give an orthorhombic cell, but monoclinic symmetry. It can be seen from Fig. 6 that the Bi-atom columns in the two neighbouring layers are not directly superposed. Such small displacements are generally observed on HRTEM images for $Bi_2Sr_2CaCu_2O_{8+\delta}$.

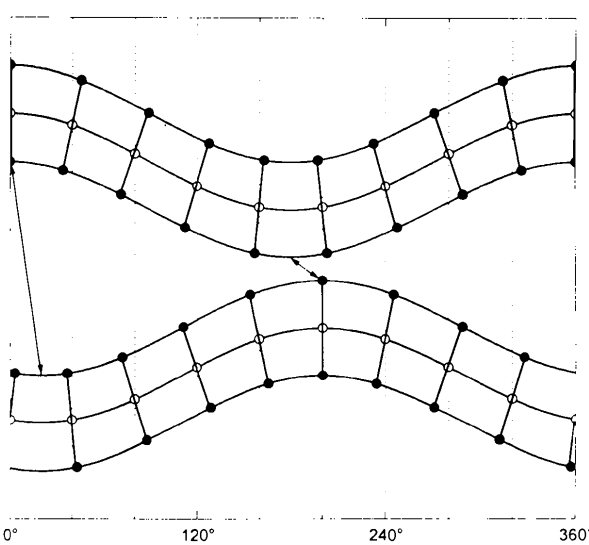

Fig. 6. Stacking of two structural slabs containing an odd number of atom columns, represented by circles, per translation unit of the corrugation. The maxima and minima of the transverse displacement waves are indicated by arrows.

3.4. *BiO layers*

The origin of the displacive modulation in the $Bi_2Sr_2Ca_{n-1}Cu_nO_{4+2n+\delta}$ structure series is generally attributed to the mismatch between the translation lattices of the BiO and the CuO_2 layers, implying – as its cause or as a possible consequence – the insertion of additional O atoms in the former. Considering a Cu—O distance of 1.9 Å, a translation unit of 5.4 Å, similar to the value observed for the $Bi_2Sr_2CaCu_2O_{8+\delta}$ structure, is obtained for the square-mesh CuO_2 layer. A regular rocksalt-type atom arrangement with the same translation unit for the BiO layer would result in unrealistic Bi—O distances of 2.7 Å. It has been proven by different experimental methods that the Bi atoms are mainly present as Bi^{III} with a lone-electron pair in this class of compounds (*e.g.* Schweizer, Müller & Gauckler, 1994). A model has been proposed, and confirmed by several refinements, where the atom arrangement in the BiO layers periodically changes between two extreme situations (Le Page, McKinnon, Tarascon & Barboux, 1989; Hewat, Capponi & Marezio, 1989), which are compared in the upper part of Fig. 7. In the Bi-rich regions corresponding to the 'inner curves' of the corrugated slab in Fig. 5, a rocksalt-type arrangement can almost be produced. In the Bi-poor regions the O atoms will move towards a bridging position between two Bi atoms, in order to obtain shorter Bi—O distances. The displacements are such that Bi—O zigzag chains are formed. Each Bi atom in the zigzag region has three close O neighbours, of which two are part of the chain and the third is situated in the neighbouring SrO layer. The lone-electron pair completes an almost perfect BiO_3 ψ-tetrahedron. When some O atoms are displaced in one direction along the chain, and others in the opposite direction, O-poor regions appear (see Fig. 7). The displacements are of such magnitude that it becomes possible to insert an additional O atom in a bridging position between the Bi atoms. Two different local symmetries may occur (Tarascon, Le Page & McKinnon, 1990): a mirror plane through a Bi atom, in which case the O sites on each side of the mirror plane can be considered as the result of the splitting of the

intermediate rocksalt position, or a twofold axis through the additional O atom. The former symmetry is observed in $Bi_2Sr_2CoO_x$, the latter in $Bi_{10}Sr_{15}Fe_{10}O_{46}$ and $Bi_8Sr_8Mn_4O_{25.5}$ (Tarascon, Le Page & McKinnon, 1990). It is possible to consider the process in the opposite sense and the displacive modulation as the consequence of the insertion of additional O atoms in the Bi—O chains. Partly or fully occupied O sites between the chains in the Bi-poor regions have also been reported for orthorhombic $Bi_2Sr_2CaCu_2O_{8+\delta}$ (Yamamoto *et al.*, 1990; Levin, Smolin & Shepelev, 1994).

Fig. 8 shows one translation unit of the infinite Bi—O chains in the two crystallographically independent BiO layers marked with *A* and *B'* in Fig. 3, in projections perpendicular to the layers and along [010]. The distances between Bi atoms belonging to the same chain are shorter than those between Bi atoms of different chains and vary from 3.5 Å in the Bi-rich regions [d(Bi(4*A*)—Bi(5*A*)) = 3.48 Å in layer *A*, d(Bi(9*B*)—Bi(1*B*)) = 3.49 Å and d(Bi(1*B*)—Bi(2*B*)) = 3.50 Å in layer *B*] to 3.9 Å in the Bi-poor regions [d(Bi(1*A*)—Bi(2*A*)) = 3.85 Å and d(Bi(4*B*)—Bi(5*B*)) = 3.89 Å]. One additional O site per translation unit of the modulation wave was found in each BiO layer. The actual composition of these layers, also hereafter referred to as BiO, is Bi_9O_{10}. In agreement with the model discussed above, the additional sites are located in the Bi-poor regions. Bi—O distances of up to 2.75 Å are indicated as stick bonds, distances between 2.75 and 3 Å by thin lines in Fig. 8, and it is possible to recognize the periodic change from the zigzag chains of corner-linked ψ-tetrahedra in the Bi-poor regions to the rocksalt-type atom arrangment in the Bi-rich regions. The list of the interatomic distances in Table 7 confirms the increase of the coordination number of Bi atoms when going from the zigzag to the rocksalt-type region, despite the poor precision of the oxygen positions which is to be expected from X-ray diffraction data. Bi(1*A*), for example, which is situated in the heart of the zigzag region, has short distances to the two O atoms of the chain ('split' positions; 2.17 and 2.30 Å) and to a third O atom, situated in the SrO layer (2.51 Å). The two next nearest O atoms are from the neighbouring BiO layer at a distance of 3.26 Å. The longest distances from a Bi atom to its O neighbour in the SrO layer are observed in this part of the structure which corresponds to the 'outer' curve of the corrugated slab. Moreover, Bi(5*A*) and Bi(6*A*), situated in the rocksalt-type region, have four O atoms at distances shorter than 2.7 Å: three O atoms from the chain and one O atom from the SrO layer. The layer *B* presents similar features with a clear threefold coordination for Bi(5*B*), Bi(6*B*) and Bi(7*B*) and a higher coordination number for the remaining sites. Bi(5*B*) shows, like Bi(1*A*) and Bi(2*A*), a longer distance to the O atom of the SrO layer than the other sites (2.45 Å), however, a very short distance of 1.84 Å was found for site Bi(6*B*). The shortest interchain distances are observed in the rocksalt-type regions of layer *B* [d(Bi(2*B*)—O(2*B*)) = 2.89 Å, d(Bi(9*B*)—O(10*B*)) = 2.94 Å].

There are no Bi—O interlayer distances shorter than 3 Å. The distances between Bi atoms of layer *A* and O atoms of layer *B* are systematically shorter than the distances between Bi atoms of layer *B* and O atoms of layer *A*. The shortest interlayer distances are found both in the Bi-rich and Bi-poor regions [d(Bi(5*A*)—O(1*B*)) = 3.10 Å, d(Bi(9*A*)—O(5*B*)) = 3.08 Å]. Additional O

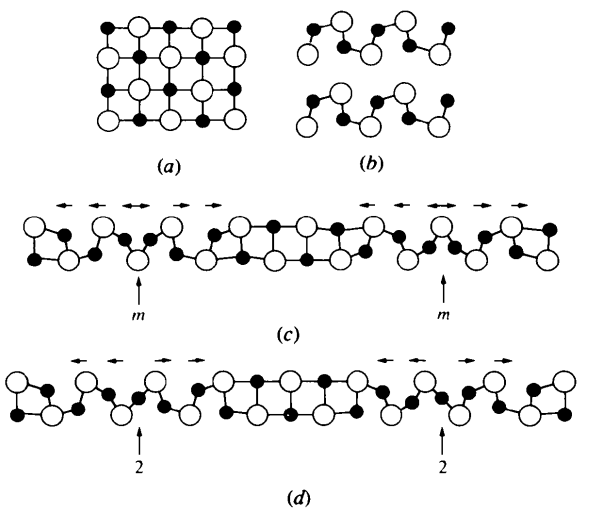

Fig. 7. Idealized atom arrangements for the BiO layers: (*a*) rocksalt-type arrangement, (*b*) infinite chains of corner-linked BiO_3 ψ-tetrahedra, (*c*) splitting of a rocksalt position leading to local mirror plane symmetry between the O sites and (*d*) insertion of an additional O atom leading to local twofold axial symmetry through the O site.

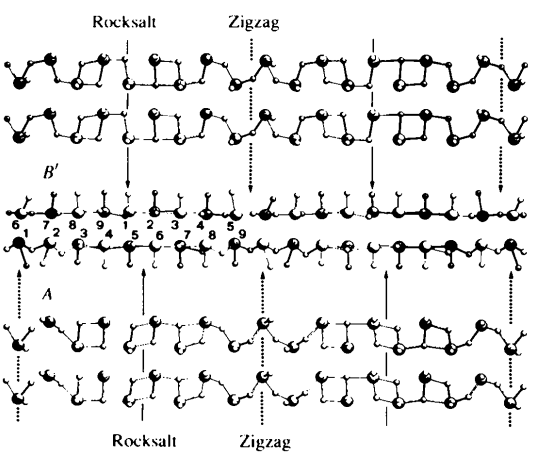

Fig. 8. Atom arrangement in the BiO layers *B'* and *A* in projections perpendicular to the layers and along [010] of the monoclinic cell (central part). The O atoms of the neighbouring SrO layers are included. Bi atoms are represented by large circles, O atoms by small circles. Stick bonds indicate Bi—O distances up to 2.75 Å, thin lines Bi—O distances between 2.75 and 3 Å. The different regions considered here are indicated by arrows.

sites were not detected either between the Bi—O chains or between the BiO layers.

Despite their great similarity, due to the relative shift of the modulation waves, slight differences are observed between the two crystallographically independent BiO layers. In layer *A* the maximum of the transverse displacement wave, which is situated at a Bi-atom column, corresponds to the zigzag region. In this layer one will expect to find an even number of O atoms in bridging positions, as in Fig. 7(*c*). It can be seen from the projection in the lower part of Fig. 8 that this is effectively the case. In layer *B*(*B'*), where the minimum of the wave corresponds to the zigzag region and goes between two Bi-atom columns, *i.e.* approximately through site O(6*B*), there is an odd number of O atoms in bridging positions, as in Fig. 7(*d*).

It has been shown by ^{17}O NMR that it is the O atoms in the BiO layers which exchange most easily (Farnan, Lombardo, Stebbins & Kapitulnik, 1994). It is plausible to postulate the existence of vacancies on the O sites in the Bi-poor zigzag region, presumably on the 'additional' sites. Unfortunately, it is not possible with the present data to test for a partial occupation of the O sites, but it cannot be excluded that the two BiO layers also have slightly different compositions. The site Bi(1*A*) and the neighbouring site in layer *B*, Bi(6*B*), show large atomic displacement parameters, with the maximum component being in the direction of the Bi—O chains. Approximately 5% vacancy was found by refinement on both sites, but as the displacement parameters remain high this may rather reflect the displacement of the Bi atoms in the presence of a neighbouring vacant O site.

The transverse and longitudinal displacements of the O sites are shown in Fig. 9. The longitudinal displacement of the O atoms of the BiO layers from the ideal rocksalt positions is conveniently described by a saw-shaped function (Petricek, Gao, Lee & Coppens, 1990). The 'additional' O sites [O(1*A*) or O(10*A*) in layer *A*, O(6*B*) in layer *B*] are situated near the discontinuity in this linear function. Atom sites O(10*A*) and O(6*B*) are considered twice in the figure (circles with an inscribed cross), calculating the displacements from the rocksalt position on either side in the chain. The linear increase of the displacement indicates that the O atoms in the BiO layers are arranged with approximately equal spacing in this direction. This has led some authors to consider the structures of the $Bi_2Sr_2Ca_{n-1}Cu_nO_{4+2n+\delta}$ structure series as an (incommensurate) intergrowth of two interpenetrating modulated substructures, the first formed exclusively by the O atoms of the BiO layers and the second by all other atoms (Walker & Que, 1992; Yamamoto, Takayama-Muromachi, Izumi, Ishigaki & Asano, 1992). In a simplified model the translation period of the square-mesh CuO_2 layer (5.4 Å) should be compared, not with that of a BiO rocksalt-type arrangement, but with the translation period of the O-atom substructure in the BiO layers (4.9 Å) to obtain an estimated value of the modulation periodicity. For the structure reported here the translation lattices coincide after nine units of the CuO_2 substructure and ten units of the substructure formed by the O atoms in the BiO layers. For the related structure containing Fe^{III}, the radius of which is slightly smaller than that of Cu^{II}, ten translation units of the FeO_2 substructure correspond to 11 units of the O substructure.

3.5. *CuO_2 layers*

The high-T_c superconductivity observed for most members of the structure series is mainly associated with the CuO_2 layers. These layers in monoclinic $Bi_2Sr_2CaCu_2O_{8+\delta}$ are shown in projections perpendicular to the layers and along [010] in Fig. 10. The Cu atoms are mainly present as Cu^{II}, inside elongated square pyramids formed by five O atoms. The average Cu—O distance within the square-mesh CuO_2 nets is 1.94 Å for

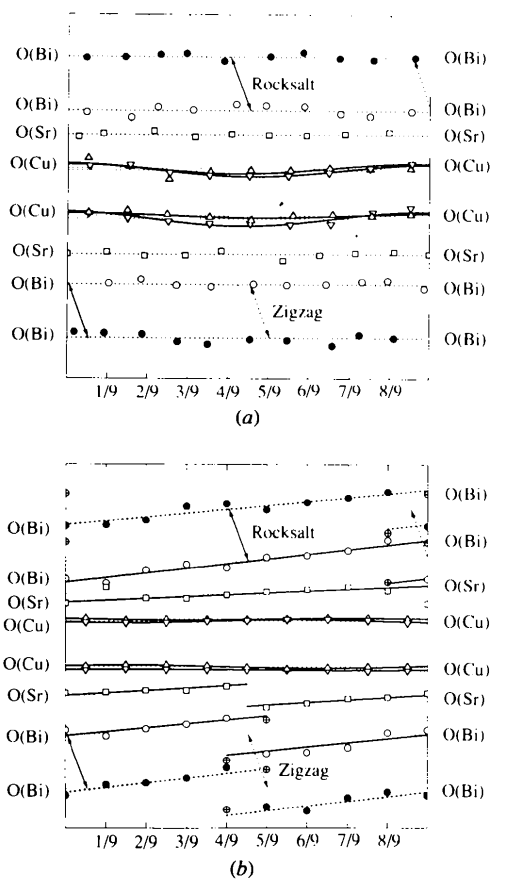

Fig. 9. Displacements of the O atoms from ideal rocksalt and perovskite positions (*a*) perpendicular to the atom layers and (*b*) parallel to the modulation direction. Atom sites in the asymmetric unit indicated in Fig. 3 are represented by open symbols, O sites from the neighbouring BiO layers *B'* and *A'* by filled circles. Circles with an inscribed cross represent the 'additional' O sites for which displacements from both neighbouring ideal rocksalt positions are considered.

both layers, with a maximum difference between the shortest and the longest bond of 0.26 Å. As mentioned above, the Cu atoms show a large amplitude for the transverse displacement, whereas the longitudinal displacement is considerably less. It can be seen from Fig. 9 that the best-fitting simple sinusoidal curves for the displacement of the O atoms in these layers are similar to those obtained for the Cu atoms, even if relatively large deviations from the curves are observed.

The distances from the Cu atoms to the apical O atoms, situated in the SrO layers, are considerably longer than the distances to the O atoms forming the square base. The average distance to the apical atom is 2.47 Å for layer *A* and 2.49 Å for layer *B*, however, there is a large variation along the modulation direction. The shortest distances correspond to the Bi-poor zigzag regions [d(Cu(1*A*)—O(11*A*)) = 2.12 Å in layer *A*, d(Cu(5*B*)—O(15*B*)) = 2.09 Å in layer *B*]. As mentioned above, the O atoms in the SrO layers also belong to the coordination sphere of the Bi atoms and constitute the connection between the two more tightly bonded parts of the structure. Except for the atom sites situated next to the zigzag regions of the BiO layers, these atoms have shorter distances to the Bi than to the Cu atom. It can be seen from Fig. 10 that in layer *B* the apical O atoms move apart from each other near the Bi-poor zigzag region. This can be interpreted as a consequence of the insertion of an additional O atom in the Bi—O chains. The corrugation of the square-mesh CuO_2 net allows the Cu atoms to maintain a pyramidal coordination with the apical O atom situated approximately on the normal to the square base. It can be noted that the distance from Cu(5*B*) to the apical O atom is relatively short (2.09 Å), whereas the corresponding distance from Cu(6*B*) is relatively long (2.70 Å). The surprisingly long distance in this region is directly related to the short Bi—O distance mentioned above, which implies the same O site. The behaviour of the apical O atoms coordinated to the Cu sites of layer *A* is slightly different. The O atoms belonging to the square pyramids of the sites Cu(1*A*) and Cu(2*A*), situated near the zigzag region, move towards each other. These pyramids, which contain the shortest distances from the central Cu atom to an apical O atom (2.12 and 2.21 Å, respectively), are strongly distorted. One of the two short O—O distances in the structure is observed between one of these sites and an 'additional' O site in the BiO layer [d(O(12*A*)—O(1*A*)) = 2.07 Å]. The displacement of the two apical O atoms towards each other could indicate partial vacancies on the 'additional' O site, but it must be kept in mind that there is doubt about the determination of the oxygen positions. The second O—O distance of the same length is observed in the same part of the structure, inside the Bi—O chain [d(O(2*A*)—O(3*A*)) = 2.07 Å]. The remaining CuO_5 square pyramids in layer *A* are tilted in a similar way to those in layer *B*.

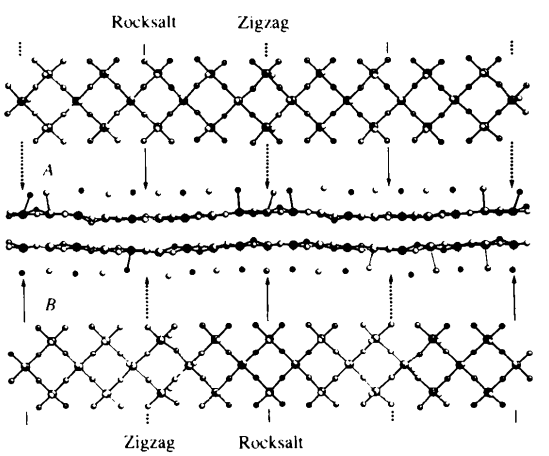

Fig. 10. Atom arrangement in the CuO_2 layers *A* and *B* in projections perpendicular to the layers and along [010] of the monoclinic cell (central part). The O atoms of the neighbouring SrO layers are included. Cu atoms are represented by large circles, O atoms by small circles. Stick bonds indicate Cu—O distances up to 2.3 Å, thin lines Cu—O distances between 2.3 and 2.8 Å. The different regions of the BiO layers considered here are indicated by arrows.

The superconductivity is related to the existence of hole carriers in the CuO_2 layers. The holes are created by excess O atoms over the stoichiometry 2-2-1-2-8, and/or by vacancies on the cation sites. A charge balance calculation made from the refined composition $Bi_{2.09}Sr_{1.90}Ca_{1.00}Cu_2O_{8.22}$, considering Bi to be trivalent, gives an average valence of 2.19 for Cu. It must be emphasized that the two CuO_2 layers, which are separated by a very slightly distorted square-mesh layer of Ca atoms, are crystallographically independent and it cannot be excluded that they contribute differently to the superconductivity.

3.6. *Ca and SrO layers*

The Ca and SrO layers are shown in two perpendicular projections in Figs. 11 and 12, where the O atoms from the neighbouring layers have also been included. The Ca-atom layer is situated in the middle of the corrugated oxygen-deficient perovskite-derived slab and the displacement of the Ca atoms from the ideal positions has a large transverse but no longitudinal component. The maxima and minima of the transverse displacement wave correspond to the zigzag region of the BiO layer on one side, but to the rocksalt-type region on the other side of the Ca-atom layer. The tetragonal prisms formed by the O atoms from the CuO_2 layers around the Ca sites are slightly distorted with an average Ca—O distance of 2.51 Å.

All O sites in the structure participate in the coordination polyhedra of the Sr sites. In the ideal structure of $Bi_2Sr_2CaCu_2O_{8+\delta}$ the Sr atoms are situated inside monocapped square antiprisms formed by four O atoms from the SrO layer, four O atoms from the CuO_2

layer and one O atom from the BiO layer. In order to obtain interatomic distances of approximately the same length to all surrounding atoms, the Sr atoms are expected to move out of the plane formed by the O atoms of the SrO layer, towards the CuO_2 and away from the BiO layer. This general tendency is well seen from the projection of the structure in Fig. 3. Relatively regular monocapped square antiprisms are observed for the sites situated near the rocksalt-type regions of the BiO layers with Sr—O distances ranging from 2.4 to 3.1 Å, see for example Sr(5*A*) and Sr(9*B*) in Table 7. The coordination number can be expected to be higher for the sites situated near the zigzag regions since two O atoms in a bridging position in the BiO layers, instead of one in a rocksalt position, cap the large square face of the antiprism. This is the case for site Sr(1*A*), for example, which has ten O atoms at distances shorter than 3.1 Å, among which two O atoms are from the BiO layer [d(Sr(1*A*)—O(10*A*)) = 2.42 Å, d(Sr(1*A*)—O(1*A*)) = 2.55 Å]. It can be seen, however, from Fig. 12 that the SrO layers are extended in this part of the structure and the site Sr(5*B*), which is also situated near the zigzag region, has only eight neighbours in the same range of interatomic distances. On average, the Sr—O distances in layer *A* are shorter than the Sr—O distances in layer *B*. It is shown in Fig. 9 that the longitudinal displacement of the O atoms in the SrO layer may also be described by a saw-shaped function, with the discontinuity in the linear function being in the same region as that of the O atoms in the BiO layers.

Results from synchrotron anomalous scattering at the Bi absorption edge (Lee *et al.*, 1989; Coppens, Lee, Gao & Sheu, 1991) have indicated that the excess Bi is to be found both on the Ca and on the Sr sites. Substitution of Ca by Bi is considered to have a positive effect on the superconductivity by reducing the distance between the two CuO_2 layers. No real evidence for a selective substitution within the Ca layers in orthorhombic $Bi_2Sr_2CaCu_2O_{8+\delta}$ has yet been reported. Ezrahni, Suresh Babu, Brohan, Tilley & Ganne (1993) suggest that Bi will preferentially substitute for Ca on Wyckoff position 4(*f*) in space group *Pnnn* in a fivefold supercell. Levin, Smolin & Shepelev (1994) consider a partial substitution of Ca by Sr for a refinement in the same cell and space group. No substitution was reported on the site in Wyckoff position 4(*f*), but the highest substitution (64% Sr) on the eightfold Ca site is situated near the zero amplitude of the transverse displacement wave.

An average value of 9.7% Bi was found on the Ca sites refined in the monoclinic superstructure reported here. This corresponds to the replacement of every 9th or 10th Ca atom by a Bi atom, however, the Bi atoms were found to be more or less regularly distributed on all Ca sites in the monoclinic supercell. A slight maximum is observed for sites Ca(4), [Ca(5)] and Ca(6), which are located in a part of the structure which corresponds to the rocksalt-type region of the BiO layer *A* and to the zigzag region of the BiO layer *B*.

A partial substitution by Ca was observed for two Sr sites which showed particularly high displacement parameters [Sr(1*A*) and Sr(6*B*)]. These two sites are situated next to the zigzag regions where the 'additional' O atoms are to be found, which confirms the idea of a local disorder in this part of the structure. The complexity of the structure did not allow us from the present X-ray diffraction data to consider a simultaneous substitution by several elements or a combination of substitution and vacancies. Partial vacancies on these sites, as reported by some authors (Beskrovnyi, Dlouhá, Jirák, Vratislav & Pollert, 1990; Beskrovnyi, Dlouhá, Jirák & Vratislav, 1990; Levin, Smolin & Shepelev, 1994), cannot be excluded, nor can a slight substitution by Bi on some Sr sites, as expected from the anomalous dispersion

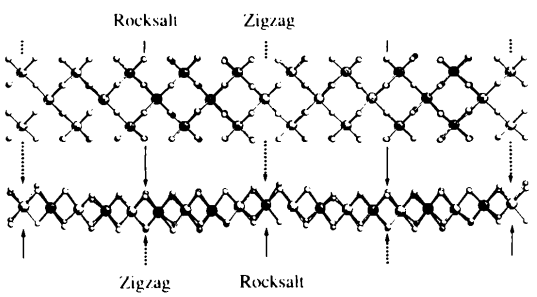

Fig. 11. Atom arrangement in the Ca layer in projections perpendicular to the layer (upper part) and along [010] of the monoclinic cell (lower part). The O atoms of the neighbouring CuO_2 layers are included. Ca atoms are represented by large circles, O atoms by small circles. Stick bonds indicate Ca—O distances up to 2.9 Å. The different regions of the BiO layers considered here are indicated by arrows.

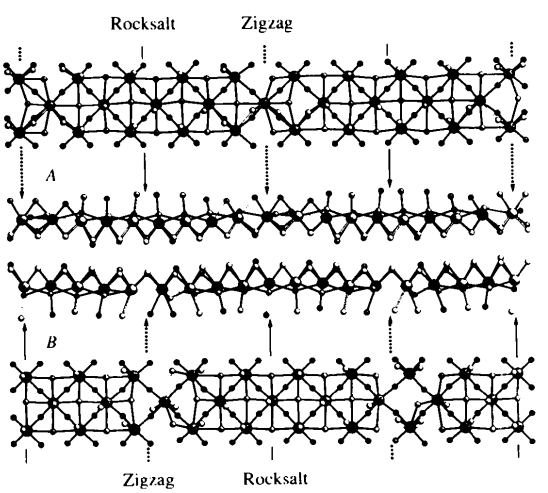

Fig. 12. Atom arrangement in the SrO layers *A* and *B* in projections perpendicular to the layers and along [010] of the monoclinic cell (central part). The O atoms of the neighbouring CuO_2 and BiO layers are included. Sr atoms are represented by large circles, O atoms by small circles. Stick bonds indicate Sr—O distances up to 3.2 Å, thin lines Sr—O distances between 3.2 and 3.5 Å. The different regions of the BiO layers considered here are indicated by arrows.

experiments quoted above. The refined composition $Bi_{2.09}Sr_{1.90}Ca_{1.00}Cu_2O_{8.22}$ is in relatively good agreement with the nominal composition $Bi_{2.16}Sr_{1.94}Ca_{1.04}Cu_2O_x$ and the composition $Bi_{2.14}Sr_{1.87}Ca_{0.99}Cu_2O_{8.15}$ as determined by a chemical analysis.

3.7. *Monoclinic $Bi_2Sr_2CuO_{6+\delta}$*

The structures of the $Bi_2Sr_2Ca_{n-1}Cu_nO_{4+2n+\delta}$ structure series have a strong two-dimensional character with only weak links between neighbouring BiO layers. A multitude of faults in the stacking of the slabs delimited on each side by a BiO layer have been observed in electron microscope images, *e.g.* a rotation of consecutive slabs by 90 or 45° (Eibl, 1990), a translation by half the short translation unit or a small translation in the modulation direction (Budin, Eibl, Pongratz & Skalicky, 1993). Matsui & Horiuchi (1988) suggested that structures with different phase shifts of the modulation waves of the two neighbouring BiO layers may form. In the orthorhombic structure reported for $Bi_2Sr_2CaCu_2O_{8+\delta}$ the longitudinal waves of the Bi atoms in two neighbouring BiO layers are in phase and, consequently, the transverse waves out of phase. For the monoclinic structure reported here we have shown above that the phase difference between the transverse displacement waves of the metal atoms in consecutive slabs is not π but $10\pi/9 \equiv 200°$. A higher value of the phase shift, $7\pi/5 \equiv 252°$, is observed for the monoclinic modification of $Bi_2Sr_2CuO_{6+\delta}$ (Onoda & Sato, 1988; Leligny, Durčok, Labbe, Ledesert & Raveau, 1992; Beskrovnyi *et al.*, 1994). The stacking of structural slabs delimited by BiO layers in the two structures is compared in Fig. 13. Dashed lines are drawn through the zero amplitude contour of consecutive transverse displacement waves. In monoclinic $Bi_2Sr_2CaCu_2O_{8+\delta}$ reported here the straight line describing the progressive phase shift forms an angle of 94.95° with the layers. The corresponding angle observed for monoclinic $Bi_2Sr_2CuO_{6+\delta}$ exceeds 110° (β angle of the monoclinic cell). It can be noted that the amplitude of the transverse displacement wave decreases with increasing thickness of the slabs.

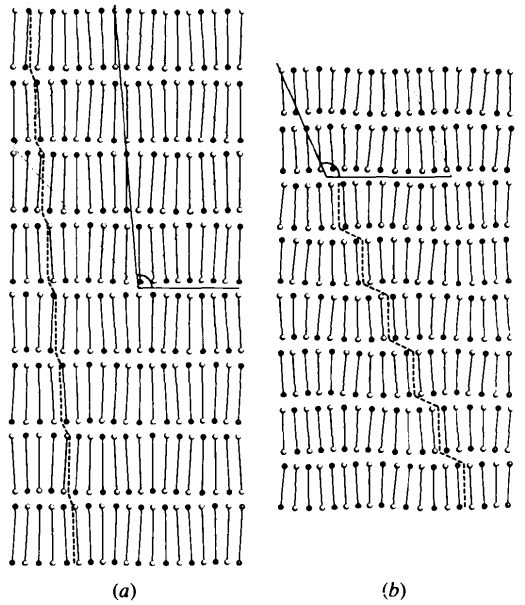

(*a*) (*b*)

Fig. 13. Stacking of structural slabs delimited on each side by a BiO layer in (*a*) monoclinic $Bi_2Sr_2CaCu_2O_{8+\delta}$ and (*b*) monoclinic $Bi_2Sr_2CuO_{6+\delta}$, in projections along [010]. Bi atoms are indicated by circles and connected by solid lines through the slabs. The dashed lines correspond to zero amplitude of the transverse displacement waves.

We thank Mr T. Tsukamoto for providing single crystals of $Bi_2Sr_2CaCu_2O_{8+\delta}$, Dr K. Cenzual for useful discussions and Dr H. D. Flack for critical reading of the manuscript. This work was supported by the Swiss National Science Foundation.

References

Beskrovnyi, A. I., Dlouhá, M., Jirák, Z. & Vratislav, S. (1990). *Physica C*, **171**, 19–24.

Beskrovnyi, A. I., Dlouhá, M., Jirák, Z., Vratislav, S. & Pollert, E. (1990). *Physica C*, **166**, 79–86.

Beskrovnyi, A. I., Durčok, S., Hejtmánek, J., Jirák, Z., Pollert, E. & Shelkova, I. G. (1994). *Physica C*, **222**, 375–385.

Blanc, E., Schwarzenbach, D. & Flack, H. D. (1991). *J. Appl. Cryst.* **24**, 1035–1041.

Budin, H., Eibl, O., Pongratz, P. & Skalicky, P. (1993). *Physica C*, **207**, 208–224.

Calestani, G., Francesconi, M. G., Salsi, G., Andreetti, G. D. & Migliori, A. (1992). *Physica C*, **197**, 283–298.

Calestani, G., Rizzoli, C., Francesconi, M. G. & Andreetti, G. D. (1989). *Physica C*, **161**, 598–606.

Coppens, P., Lee, P., Gao, Y. & Sheu, H. S. (1991). *J. Phys. Chem. Solids*, **52**, 1267–1272.

Eibl, O. (1990). *Physica C*, **168**, 239–248.

Ezrahni, M., Suresh Babu, D., Brohan, L., Tilley, R. J. D. & Ganne, M. (1993). *Int. J. Modern Phys. B*, **7**, 151–156.

Farnan, I., Lombardo, L. W., Stebbins, J. F. & Kapitulnik, A. (1994). *Physica C*, **232**, 27–36.

Gao, Y., Coppens, P., Cox, D. E. & Moodenbaugh, A. R. (1993). *Acta Cryst.* A**49**, 141–148.

Gao, Y., Lee, P., Coppens, P., Subramanian, M. A. & Sleight, A. W. (1988). *Science*, **241**, 954–956.

Hall, S. R., Flack, H. D. & Stewart, J. M. (1992). Editors. *Xtal3.2 User's Guide*. Universities of Western Australia, Australia, Geneva, Switzerland, and Maryland, USA.

Hewat, E. A., Capponi, J. J. & Marezio, M. (1989). *Physica C*, **157**, 502–508.

Horiuchi, S., Maeda, H., Tanaka, Y. & Matsui, Y. (1988). *Jpn. J. Appl. Phys.* **27**, L1172–L1174.

Junod, A., Wang, K. Q., Tsukamoto, T., Triscone, G., Revaz, B., Walker, E. & Muller, J. (1994). *Physica C*, **229**, 209–230.

Kan, X. B. & Moss, S. C. (1992). *Acta Cryst.* B**48**, 122–134.

Le Page, Y., McKinnon, W. R., Tarascon, J. M. & Barboux, P. (1989). *Phys. Rev. B*, **40**, 6810–6816.

Lee, P., Gao, Y., Sheu, H. S., Petricek, V., Restori, R., Coppens, P., Darovskikh, A., Phillips, J. C., Sleight, A. W. & Subramanian, M. A. (1989). *Science*, **244**, 62–63.

Leligny, H., Durčok, S., Labbe, P., Ledesert, M. & Raveau, B. (1992). *Acta Cryst.* B**48**, 407–418.

Levin, A. A., Smolin, Yu. I. & Shepelev, Yu. F. (1994). *J. Phys. Condens. Matter*, **6**, 3539–3551.

Maeda, H., Tanaka, Y., Fukotomi, M. & Asano, T. (1988). *Jpn. J. Appl. Phys.* **27**, L209–L210.

Matsui, Y. & Horiuchi, S. (1988). *Jpn. J. Appl. Phys.* **27**, L2306–L2309.

Niu, H., Fukushima, N., Takeno, S., Nakamura, S. & Ando, K. (1989). *Jpn. J. Appl. Phys.* **28**, L784–L786.

Onoda, M. & Sato, M. (1988). *Solid State Commun.* **67**, 799–804.

Onozuka, T. & Hirotsu, Y. (1994). *Acta Cryst.* A**50**, 231–238.

Patterson, C., Hatton, P. D., Nelmes, R. J., Chu, X., Yan, Y. F. & Zhao, Z. X. (1990). *Supercond. Sci. Technol.* **3**, 297–301.

Petricek, V., Gao, Y., Lee, P. & Coppens, P. (1990). *Phys. Rev. B*, **42**, 387–392.

Schweizer, T., Müller, R. & Gauckler, L. J. (1994). *Physica C*, **225**, 143–148.

Takenaka, H., Kamigaki, K., Terauchi, H. & Katsui, A. (1989). *J. Phys. Soc. Jpn*, **58**, 775–778.

Tarascon, J. M., Le Page, Y. & McKinnon, W. R. (1990). *Eur. J. Solid State Inorg. Chem.* **27**, 81–104.

Tsukamoto, T., Triscone, G., Genoud, J. Y., Wang, K. Q., Janod, E., Junod, A. & Muller, J. (1994). *J. Alloys Comp.* **209**, 225–229.

Walker, M. B. & Que, W. (1992). *Phys. Rev. B*, **45**, 8085–8090.

Yamamoto, A., Onoda, M., Takayama-Muromachi, E., Izumi, F., Ishigaki, T. & Asano, H. (1990). *Phys. Rev. B*, **42**, 4228–4239.

Yamamoto, A., Takayama-Muromachi, E., Izumi, F., Ishigaki, T. & Asano, H. (1992). *Physica C*, **201**, 137–144.

Zachariasen, W. H. (1968). *Acta Cryst.* A**24**, 212–216.

Zhigadlo, N. D. (1994). *J. Phys. Condens. Matter*, **6**, 8969–8975.